Summer 2014

The effect of arch insoles on tibial rotation and tibiofemoral contact stress

Saphia Fatima Waheed
University of Iowa

Recommended Citation

Waheed, Saphia Fatima. "The effect of arch insoles on tibial rotation and tibiofemoral contact stress." MS (Master of Science) thesis, University of Iowa, 2014.
http://ir.uiowa.edu/etd/2160.

THE EFFECT OF ARCH INSOLES ON TIBIAL ROTATION AND TIBIOFEMORAL
CONTACT STRESS

by

Saphia Fatima Waheed

A thesis submitted in partial fulfillment
of the requirements for the Master of
Science degree in Biomedical Engineering
in the Graduate College of
The University of Iowa

August 2014

Thesis Supervisor: Associate Professor Neil Segal

Graduate College
The University of Iowa
Iowa City, Iowa

CERTIFICATE OF APPROVAL
_____

MASTER'S THESIS

_____

This is to certify that the Master's thesis of

Saphia Fatima Waheed

has been approved by the Examining Committee
for the thesis requirement for the Master of Science degree
in Biomedical Engineering at the August 2014 graduation.

Thesis Committee: _____
                      Neil Segal, Thesis Supervisor

                      _____
                      Donald Anderson

                      _____
                      Nicole Grosland

ACKNOWLEDGMENTS

TABLE OF CONTENTS

LIST OF TABLES

Table

LIST OF FIGURES

Figure

CHAPTER 1: INTRODUCTION

1.1 Background and Rationale

Approximately 21% of American women will experience knee pain at some point

in their lives, and over 19% of American women will experience knee osteoarthritis

during their lifetime [1, 2]. It is estimated that joint pain and disability due to

osteoarthritis costs the United States about $128 billion dollars annually, and knee

replacements due to pain-induced disability cost the United States about $29 billion every

year [2, 3]. This statistic includes health care costs, but overlooks other costs such as lost

employer productivity and personal income. With the increasing amount of women

experiencing knee pain, research is needed to create preventative solutions for patients to

limit their chances of developing knee pain.

One condition that could contribute to women being disproportionally affected by

knee pain and osteoarthritis compared with men is a decrease in foot arch height that

persists following pregnancy [4]. A reduction in arch height during pregnancy likely

relates to increased body mass, increased circulation of hormones, and increased joint

laxity. A previous study found that women may lose arch height of 1-5 mm in their feet

while they are pregnant. This change in arch height persists at 19 weeks post-partum and

is thought to be permanent [5]. Although it has been determined that there are changes in

the arches of the feet that develop throughout pregnancy, the effects of these changes

have not been studied for their impact on knee pain and knee osteoarthritis.

Several biomechanical changes can occur as a result of a drop in arch height and

subsequent foot pronation, including increased shock absorption by the foot, shift in

loading in the knees and a permanent change in the lower limb kinetic chain [5]. The

effects of these factors during weight-bearing conditions can lead to internal tibial

rotation. Internal tibial rotation can cause malalignment of the tibia and femur and

increase stress on the lateral part of the knee joint [5, 6, 7]. Many sources of knee pain,

such as knee osteoarthritis, iliotibial band friction syndrome, anterior tibial translation,

patellofemoral pain, and greater trochanteric pain syndrome, can be attributed to the

effect of internal tibial rotation [6, 7]. Knee osteoarthritis is a degenerative disease that

affects the entire joint, especially the cartilage and underlying bone. Both biological and

mechanical factors are thought to affect the progression of osteoarthritis [3, 4]. Prior

research results indicate that higher maximum contact stress at the knee joint is apparent

in subjects who suffer from knee osteoarthritis [3, 4, 7, 8].

Results of previous studies indicate that there is a correlation between contact

stress exposure and osteoarthritis development in the tibiofemoral joint [4, 8].

Measurements of contact stress exposure on articular joint surfaces are a reliable method

for examining the effect of mechanical factors involved in the development and

progression of knee osteoarthritis. Discrete element analysis (DEA) is a method of rigid

body spring modeling used to estimate contact stresses between two articulating surfaces

[8]. DEA is more time-effective than other methods because it allows many subjects to be

analyzed at once and computes only contact stress distributions and resulting reaction

forces. With DEA, the underlying bone in a joint is modeled as a rigid body and cartilage

is modeled as compressive springs. The displacement between the rigid bodies is then

used to determine deformation of the compressive springs [8]. Though this method is not

able to compute internal stresses in bone or cartilage it holds attraction for evaluating

contact stress with the goal of determining a potential correlation with internal tibial rotation due to arch drop.

1.2 <u>Study Objectives</u>

There were two main objectives of this study: (1). to evaluate change in degree of tibial rotation with and without insole support of arch height in postpartum women with flexible arches; and (2) to evaluate the effect of these conditions on tibiofemoral contact stress. The research objectives were studied to test the hypothesis that there will be an increase in a) internal rotation of the tibia and b) medial tibiofemoral articular contact stress in an arch-unsupported, compared with an arch-supported, condition in postpartum women with flexible foot arches.

CHAPTER 2: BACKGROUND

2.1 Human Foot Anatomy

The human foot is a complex structure composed of 26 bones and 112 ligaments that supports the weight of the entire body [9]. There are three primary functions of the foot: weight bearing, stability, and propulsion [9, 10]. During weight-bearing conditions, the foot absorbs shock and transfers load to the more proximal segments of the lower limb [11].

The foot can be divided into three segments: forefoot, midfoot, and hindfoot. The forefoot is composed of the metatarsal and phalanges, and the midfoot, which is located in between the forefoot and hindfoot, contains five articulating tarsal bones. The hindfoot contains the talus and calcaneus bones [9]. The talus articulates with the tibia and fibula to allow ankle dorsiflexion and plantar flexion [9]. The midfoot connects the forefoot and hindfoot with the main arch support of the foot, the longitudinal arch. As shown below in Figure 1, a second arch in the foot, the transverse arch, is located mediolaterally under the metatarsals. Both arches provide flexibility and support to the foot [12, 13]. The longitudinal arch can be divided into two parts: the medial longitudinal arch and lateral longitudinal arch. The lateral longitudinal arch is slightly less elastic than the medial longitudinal arch due to its smaller elevation [12]. Both the medial and lateral longitudinal arches are supported by ligamentous structures so that they are able to support weight-bearing [12].

The plantar fascia is a thick connective tissue that provides inferior support to the longitudinal arch [14, 15]. It originates from the medial tubercle on the calcaneus and inserts at the metatarsophalangeal joints [16]. When placed under weight-bearing

conditions, the plantar fascia absorbs tension from the ground and body to prevent arch

collapse. Damage to the longitudinal arch may decrease its ability to support arch height.

Arches of the Foot

A-B Anterior Transverse Arch
B-C Lateral Longitudinal Arch
A-C Medial Longitudinal Arch
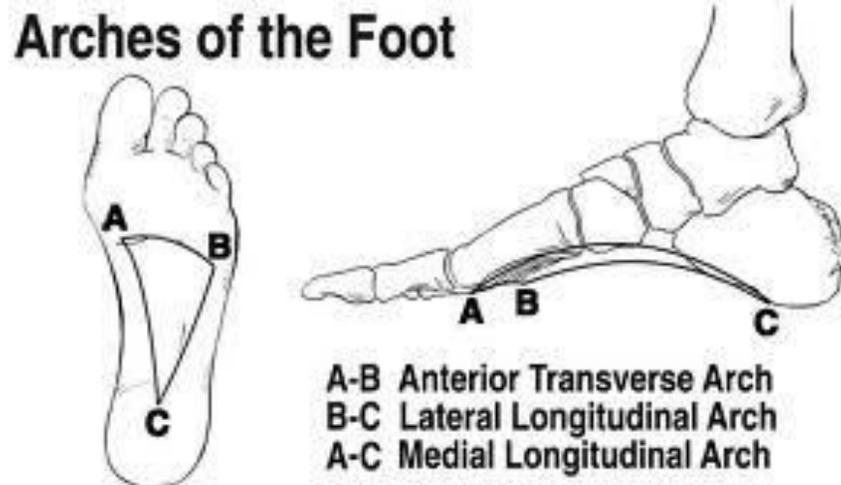
Figure 1. The medial and lateral longitudinal and transverse arches of the foot
[17].

Excessive strain to the plantar fascia can irritate or damage the tissue, causing it to

weaken to the point where it can no longer provide sufficient support to avoid arch

collapse [15]. Pes planus ("flatfoot") is a postural irregularity that results from collapse of

the longitudinal arch. This condition causes over-stretching of the plantar fascia and

development of plantar fasciitis [16]. Changes to the foot structure will change load

distribution within the foot and alter shock absorption.

2.1.1 Arch Height

There are three classifications of foot type based on arch height. Neutrally aligned

feet have no eversion or inversion of the calcaneus (heel bone) and have a normal arch

height (rectus). A normal arch height, which varies per person, is the height of the arch

during non-weight-bearing conditions if there is no calcaneal eversion or inversion. Pes cavus feet are characterized by calcaneus inversion and a high arch height. The final foot type is pes planus, which is characterized by calcaneus eversion and low arch height [10]. Calcaneal eversion causes foot pronation, which is the inward rolling of the foot. Foot pronation will reduce arch height and may lead to plantar fasciitis [10, 16].

<div align="center">2.2 Arch Drop</div>

<div align="center">*2.2.1 Pregnancy Effect on Arch*</div>

During pregnancy, women experience musculoskeletal changes that may affect their arch height [18, 5]. A reduction in arch height may be due to a variety of causes. For example, a large body mass index would place a greater stress on the longitudinal arch and cause it to compress [19]. A compressed arch will increase the contact area of the foot during weight-bearing conditions, and alter the force distribution within the foot and lower extremity [19]. Hormonal effects on the body during pregnancy may cause joint instability by increasing peripheral ligamentous laxity. Both increased body mass and hormonal changes during pregnancy can play a role in increasing ligamentous laxity, which may lead to a collapse in arch height and decrease in joint stability [5, 20, 21, 22]. Joint stability is the ability to maintain and control movement of the joint. Increased joint pain and risk of injury to surrounding joints may occur as a result of joint instability. Joint instability may increase because of pregnancy effects, old age, or joint injury [21, 22].

Research shows that there may be an increase in foot size during pregnancy because of accumulation of extra fluid or an increase in body mass [23]. Segal et al. compared measurements of foot anthropometrics for women at the beginning of their

pregnancy with post-partum measurements and found that an increase in foot length and arch drop occurs during pregnancy and persists at 19 weeks post-partum [5]. Due to an increase in volume of blood in the body, fluid for the fetus, and amniotic fluid, pregnant women retain an average of 6.5 liters of fluid during their pregnancy [23]. This fluid retention, combined with an average of 26 pounds gained during pregnancy, may affect joint laxity, leading to a decrease in arch height [5, 23]. Fluid retention alone is not accepted as a reason for joint laxity, because the fluid is mostly removed from the body early postpartum [23]. An increase in fluid may increase swelling in the foot. Though excess fluid will be eliminated after pregnancy, the foot swelling can lead to ligamentous laxity that persists beyond pregnancy. This laxity can cause the arch height to drop [23].

An increase in body mass can also affect women's posture during pregnancy. Due to the position of the fetus, there is an increase in anterior load, which affects center of pressure on the foot during gait. Previous studies have found that a change in center of pressure during gait is associated with lengthening and depressing of the longitudinal arch [5]. This change in arch occurs as a result of an increase in pressure on the midfoot of the body due to postural changes in the women's body. The change in pressure on the foot shifts some of the load from the hindfoot to the midfoot, which is supported by the longitudinal arch [9, 24].

2.2.2 Hormone Effect on Joint Laxity

Schauberger et al. found that joint laxity increases during pregnancy and remains at an elevated level postpartum [22]. Hormonal changes during pregnancy can cause joint laxity, which can then affect arch height. Relaxin is a peptide hormone that is produced by the corpus luteum in females. Though this hormone is produced in pregnant as well as

non-pregnant females, its secretion rate is highest in pregnant women [23, 25]. The effects of relaxin include inhibition of collagen synthesis and relaxation of pelvic ligaments, and increased laxity of peripheral joints [25]. Relaxation of tissues in the pelvic region prepares the body for delivery by widening the pelvis. By inhibiting collagen synthesis, relaxin may decrease the strength of ligaments and increase joint laxity [15]. This may directly affect arch height by preventing ligaments in the foot from maintaining normal arch height and cause a collapse. Serum levels of cortisol, estrogen, and progesterone may also increase during pregnancy. These hormones have also been linked to an increase in joint laxity [22].

2.2.3 Tibiofemoral Joint Pain

The effects of a decrease in arch height due to pregnancy are theorized to correlate with internal rotation of the tibia [5]. The change in position of the tibia can affect mechanical stresses at the knee. Gross et al. found a positive correlation between a decrease in arch height and the existence of knee joint pain and cartilage degeneration in older adults [26]. Increased joint laxity during pregnancy is associated with low back, hip, and knee pain that often remain after delivery [21]. Pes planus feet have been linked with abnormal plantar pressure, indicating a change in distribution of force within the foot under weight-bearing conditions [10, 17]. This may also alter force distribution in the knee, hip, and back and cause joint pain.

Foot posture and arch height affect development of lower extremity musculoskeletal disorders, and orthotic insoles may prevent collapse of arch height from creating malalignment of the knee joint [27]. Levinger et al. observed that people with medial compartment knee osteoarthritis had a more pronated foot and lower arch height

than people without knee osteoarthritis [28]. The results of this study indicate that orthotic insoles may maintain arch height during pregnancy and consequently decrease the chance of developing knee osteoarthritis [28].

<div align="center">2.3 Human Knee Anatomy</div>

The human knee is a synovial hinge joint that includes the proximal tibia and fibula, distal femur, patella, and supporting ligaments and muscles. The proximal tibia consists of a tibial plateau made up of medial and lateral condyles separated by the tibial spine (Figure 2) [29, 30]. The tibial spine is a raised bony ridge in the center of the tibial plateau that serves as a ligamentous attachment region. The tibial condyles are shaped to articulate with the corresponding condyles on the distal femur. The medial femoral and tibial condyles are larger in size than those on the lateral side [30]. The femoral condyles are able to flex and extend in the sagittal plane and rotate internally and externally in the transverse plane. The menisci are fibrocartilaginous structures, fastened to the tibial spine, which form a semi-lunar cup shape to accommodate the shape of the femoral condyles and aid with support and stability of the knee joint (Figure 3) [29]. Additional knee stabilization is provided from supporting ligaments and muscles during dynamic activity [29].
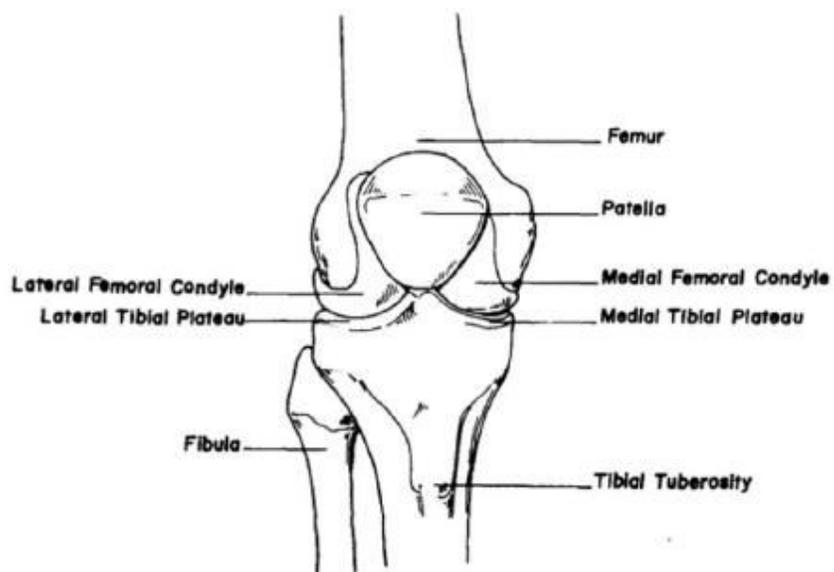
Figure 2. Knee anatomy illustrating the bones and tibial plateau [29].
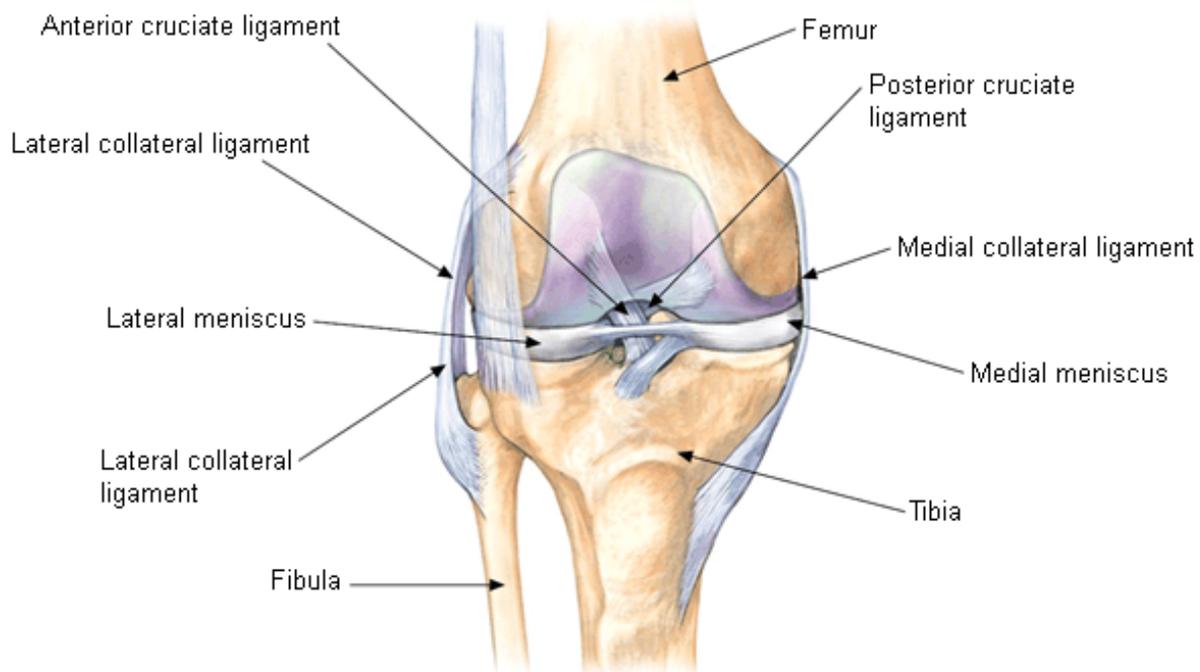
Figure 3. Knee anatomy illustrating meniscus and ligament attachment [31].

The main purpose of the tibiofemoral joint is to provide shock absorption and support the weight of the body. This di-arthrodial joint involves two main articulations: the tibiofemoral joint and patellofemoral joint [29]. The superior tibiofemoral joint connects the distal femur to the proximal tibia, enabling and supporting movement during dynamic motion. The patellofemoral joint connects the distal femur to the patella [29, 30].

Tibiofemoral anterior translation and internal rotation of the tibia is restricted by the anterior cruciate ligament (ACL) [32]. The ACL attaches to the tibial spine and is smaller in women than in men, making it more susceptible to injury. The posterior cruciate ligament, which also attaches to the tibial spine, prohibits the tibia from translating too far posteriorly in relation to the femur [29].

<u>2.4 Tibial Rotation</u>

2.4.1 Causes

The subtalar joint is an articulation between the talus and calcaneus of the human foot that allows supination and pronation of the foot to aid with dynamic movements such as walking and running (Figure 4) [33]. Subtalar joint eversion, also called foot overpronation, indicates a low arch height that elongates the foot and causes it to roll inwards [34, 35]. Because the subtalar joint more or less acts as a hinge, eversion of this joint can cause internal rotation of the tibia [35]. Subjects with pronated feet were found to have a significantly greater degree of internal tibial rotation than subjects with no pronation [34].

Overpronation of the foot can lead to valgus deformities at the knee. For example, genu valgum is a condition that causes the proximal tibia and distal femur to deviate

medially. As a result, the stresses at the knee will shift laterally, changing knee alignment and possibly causing cartilage degeneration [36].
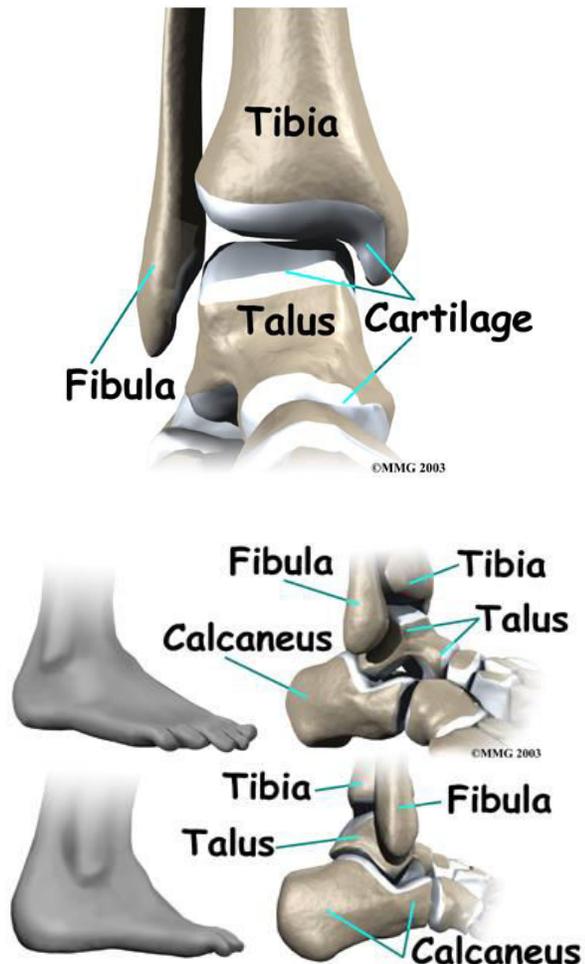
Figure 4. Anatomy of the subtalar joint showing the talus, calcaneus, and tibia [37].

Internal tibial rotation is a condition that occurs when the tibia rotates internally along its long axis. Rotation of the tibia about this axis shifts the articulation point of the tibia and femur and may increase contact stress between the two bones. Dynamic activities with a pronated foot may increase the rotation of the tibia and subsequently

increase stresses on the ACL [38]. Malalignment of the tibia and femur can lead to many lower limb disorders, including knee pain and flexion instability [33, 34]. Excess contact stress on the tibia may lead to cartilage degeneration and development of knee osteoarthritis [33, 34].

2.4.2 Impact on Musculoskeletal Disorders

Several lower extremity musculoskeletal disorders can result from internal tibial rotation, including iliotibial band friction syndrome (IBFS), patellofemoral pain, anterior tibial translation, greater trochanteric syndrome, and knee osteoarthritis.

2.4.2.1 Iliotibial Band Friction Syndrome

The iliotibial band (ITB) is a band of connective tissue that begins at the anterior iliac tubercle portion of the iliac crest and inserts at the lateral tubercle of the tibia, known as Gerdy's tubercle [39, 40]. Its related muscles function to allow extension, flexion, abduction, and medial rotation of the hip [39]. In addition, the ITB provides stability to the lateral knee during flexion and extension movements [39, 40].

IBFS is a condition caused by friction between the ITB and the lateral femoral epicondyle. This syndrome, which constitutes about 22% of lower extremity injuries, is apparent during knee extension and flexion, when the ITB is pulled more tightly at the knee [41]. Causes of IBFS include overuse of the tibiofemoral joint during dynamic movement and internal tibial rotation [41, 42]. Internal tibial rotation can force the lateral condyle of the tibia to shift anteriorly, which will increase friction of the ITB as it is pulled more tightly over the condyle during dynamic motion. IBFS can cause lateral knee joint and thigh pain and inflammation [39-42]. Treatment for IBFS includes anti-inflammatory medication, physical therapy, and arthroscopy [42].

2.4.2.2 Patellofemoral Pain

IBFS may also weaken hip adductors, causing patellofemoral pain [42, 43].

Patellofemoral pain is located at the contact area between the patella and femur. When

the hip cannot rotate externally, the knee shifts medially and the subsequent rotation of

the femur under the patella causes pain [40, 43]. Patellofemoral pain is one of the most

common types of knee pain. Because the patella attaches on the tibial tuberosity via the

patellar tendon, it may rotate along with the tibia during internal tibial rotation [40, 44,

45]. This rotation can cause malalignment of the patella and femur. Internal tibial rotation

decreases the angle that is created by the intersection of a line connecting the anterior

superior iliac spine to the midpoint of the patella and the proximal extension of a line

connecting the tibial tubercle to the midpoint of the patella. This change in angle may

decrease the lateral force acting on the patella [45]. At the same time, a tight ITB can

cause malalignment of the patella during knee flexion by forcing its movement laterally

[43, 46].

2.4.2.3 Anterior Tibial Translation

Internal tibial rotation may lead to anterior tibial translation. During internal tibial

rotation, the tibial lateral condyle is pulled anteriorly, which leads to over exertion and

stretching of the ACL. Since the ACL is the primary restraint to anterior tibial translation,

its ability to keep the tibia in position is compromised when it is weakened. Due to this

reason, the ACL may not prevent total anterior movement when the tibia is rotated

internally [47]. The effect of internal tibial translation on the ACL's ability to limit

anterior tibial translation occurs over a long period of time. Women are more likely than

men to experience ACL injuries. The ACL contains hormone receptors, so an increase in

relaxin, estrogen and progesterone hormone levels may increase laxity of this ligament [48].

<u>2.4.2.4 Greater Trochanteric Pain Syndrome</u>

Greater trochanteric pain syndrome (GTPS) is a condition that involves pain on the lateral hip and affects up to 25% of the population [49]. This syndrome is characterized by inflammation of tissues that lie over the greater trochanter on femur near the lateral hip [6, 49]. Segal et al. found a higher prevalence of GTPS in women and people with IBFS, knee osteoarthritis, or low back pain [6]. This pain can be generated from damage to nearby muscles and tissues, overuse of the hip, and ITB disorders [49, 50]. Tightening of the ITB over the greater trochanter region may explain the increase in irritation observed in that region during GTPS. Knee and back pain could cause GTPS through compensatory movements made to relieve symptoms in other lower limb regions [6, 49, 50]. GTPS and general hip joint wear may be caused by problems with supporting structures, such as the feet [6, 49]. Flat feet may alter a person's posture and affect their hip alignment, leading to GTPS. The effects of knee osteoarthritis combined with increased stresses on the hip and knee joint may also lead to the development of GTPS [6, 49].

<u>2.5 Knee Osteoarthritis</u>

Knee osteoarthritis is one of the most widespread forms of osteoarthritis. This disease is characterized by degeneration of cartilage and corresponding damage to underlying bone [51]. Excessive joint loading, malalignment and instability of the knee joint can cause injury to the articular cartilage and lead to tibiofemoral degeneration and osteoarthritis [52]. Excess friction between the articulating bones can affect the bones and

surrounding soft tissue. Knee osteoarthritis may cause pain, swelling, inflammation, and increased ligament laxity [51]. Weakened surrounding muscles may result from the pain and lax ligaments, reducing the amount of shock that is absorbed before being transferred to the bones at the joint. Knee osteoarthritis is most likely to develop in older women and increases the risk of disability and problems due to related medical complications [51, 52, 53, 54]. Risk factors for knee osteoarthritis development include joint malalignment, advanced age or weight, and other issues that would limit recovery from excessive loading. Women are at greater risk for developing knee osteoarthritis than men. Though little is known about the development and progression of knee osteoarthritis, causes of knee osteoarthritis may be injury, infection, increased weight on the knee joint, or other mechanical factors [55]. Internal tibial rotation may cause laxity of the ACL and malalignment of the tibia and femur, leading to progression of knee osteoarthritis. Another potential cause for development of knee osteoarthritis is a shift in the load bearing area, which could cause articular cartilage damage and thereby further increase joint laxity [56].

An increase in contact stress is thought to affect the onset of knee osteoarthritis by increasing wear. Contact stress may be increased due to increased forces on the knee joint or malalignment of the knee joint [51]. Other reasons for elevated contact stress include abnormal joint shape or overuse of the joint. Segal et al concluded that a link between articular contact stress and increased risk for symptomatic knee osteoarthritis development does exist [57]. Contact stresses in the knee joint are a stronger predictor of osteoarthritis than traditional anthropometric and demographic measures [57].

2.6 Discrete Element Analysis

Currently, there is no existing non-invasive methodology for determining joint contact stresses. For that reason, computational methods are used to predict joint contact stress between natural and artificial surfaces in orthopaedic biomechanics [58]. Discrete element analysis (DEA) is a computational stress analysis method used to solve in vivo articular joint contact problems [52, 59]. DEA relies on a more simplified model treatment than finite element analysis (FEA), making it more ideal to use when computing contact stresses between rigid bodies quickly in large simulations [60]. Understanding and being able to predict joint contact stress is necessary to better understand the clinical impacts that result from knee joint degeneration [58].

In DEA, articular cartilage is treated as an array of compressive springs connected to underlying bone surfaces. The bone surfaces are treated as rigid surfaces. A load or displacement is applied to the bodies, resulting in spring deformation. This deformation is used to compute contact stress between articulating bodies [8, 58, 61].

Blankevoort et al. developed an implementation of deformable contact using DEA with the assumption that the contacting surfaces are isotropic, linear-elastic, and bonded to a rigid surface [62, 63]. This model states that deformable springs are spread over the contact surface. Each compressive spring on the contact surface is considered separate from the others, with the pressure on any one spring being unaffected by the others. Therefore, contact stress is determined independently for each spring, simplifying the contact. This will reduce both the complexity and computation run-time of DEA [62, 63]. There are three assumptions made for this DEA theory. The first assumption is that the contact area size is larger than the cartilage thickness. Secondly, the cartilage is an

isotropic linear elastic material. The final assumption is that deformation of the subchondral bone is negligible [63]. Spring deformations using this contact model are converted to contact stress using a penetration analysis. With this analysis, any overlap between two contact surfaces is indicative of surface deformation [58, 64].

The DEA methodology has been validated against other computational contact stress estimation techniques. Li et al. compared the DEA methodology to FEA, a simplified elasticity model, and a modified Hertzian theory with a hip joint and concluded that all four of these methods resulted in similar contact stress predictions [59]. Non-linear and linear DEA methodology were compared with FEA models in a dynamic tibiofemoral weight-bearing task for a total knee replacement by Halloran et al [64]. Computed contact stress estimates were similar for DEA and FEA results. Nonlinear DEA was found to have a more accurate contact stress prediction and exceed the FEA computations by about 15% at peak pressure [64]. From these studies, it is clear that DEA is a comparable alternative to FEA that can compute accurate contact stress results. As described in the following chapter, this method is used to analyze changes in contact stress at the tibiofemoral joint between cases of insole-supported and unsupported arch height.

CHAPTER 3: METHODS

3.1 Subject Characteristics

Eleven previously pregnant subjects were recruited for this study, providing a total of 21 knees (1 subject had an MRI scan available for only one knee). The subjects had a mean weight of 165 pounds and their shoe sizes ranged from 7.5 to 9. The study participants were recruited if they demonstrated a lasting decrease in arch height following pregnancy or if they had a large change in arch height between standing and sitting positions. The arch height of all subjects was measured during a previous foot study conducted at the University of Iowa that measured changes in foot anthropometrics before and after a pregnancy. An assumption was made that women who had a measurable change in arch height between sitting and standing conditions during a pregnancy experienced that change due to effects of their pregnancy. Since the subject's arch height changed between the two positions, their arch was determined to be non-rigid. Medially elevated non-rigid arches are able to deform under weight-bearing conditions and directly support the longitudinal arch of the foot. Exclusion criteria for study subjects included women that were not able to undergo MRI and CT scans and women who were currently pregnant. All participants provided written informed consent before enrollment in this study. This study was approved by the University of Iowa Institutional Review Board.

3.2 Data Acquisition

For the study, a semi-rigid insole was used to raise arch height of subjects in order to compare the effects of a change in arch height. These arch supports were used to increase arch height. A Walkfit semi-rigid insole was used for this study because it

provides support to the arch during weight-bearing stance without considerable

deformation due to the weight of the subjects (Figure 5) (Walkfit Platinum, LLC, Van

Nuys, CA). Unlike flexible insoles with gel or cushioning, a semi-rigid insole provides a

sturdy and supportive base for barefoot subjects to stand on during weight-bearing CT

scans.

Figure 5. Rigid insoles used to change arch height during WBCT scans.

3.2.1 Positioning and Acquisition of Imaging

Each subject was scanned twice with the weight-bearing CT scanner (Curvebeam,

Warrington, PA). The first scan required them to wear arch insoles and the second scan

was done with the insoles removed. For each scan, the subjects were positioned in the

weight-bearing CT scanner with their heels and toes aligned to specific markings on the

platform (Figure 6). The position of the feet was maintained between both scans to observe the effect of the insoles on the knees with no interfering change in position of the feet. Once their feet were positioned properly, the subjects were asked to flex their knees until they touched a foam positioner and to lean forward until their thighs were resting against the foam positioner. The purpose of the foam positioner was to maintain a set degree of minimal knee flexion and to allow natural movement of the knees during insole removal in between scans. A stiff positioner would place the subject's knees in an uncomfortable position and may limit natural movement of the knee. As seen below in Figure 7, each subject's arms were positioned so that their elbows were in line with their body. The subjects were placed in a specific position so that the effect of the insole on tibial rotation could be measured without any interfering impacts from other parts of the body.

The weight-bearing CT scanner imaged the knees in a flexion position of approximately 15-20° to permit maximum rotational effects of the tibia. The knees were not restrained in full extension because of the difficulty of the subjects to stand still without any shift in position for the duration of both scans with both knees fully extended. After the first CT scan, the insoles were carefully removed so there was minimal adjustment on subject position. During the insole removal process, the subject remained positioned and raised one heel at a time. The insoles were removed by sliding them out from under the heel and the foot was guided back to its original position. Throughout this process, a second research assistant assessed subject positioning to ensure there was no excessive movement of the pelvic or knee region and no change in position of the foot.
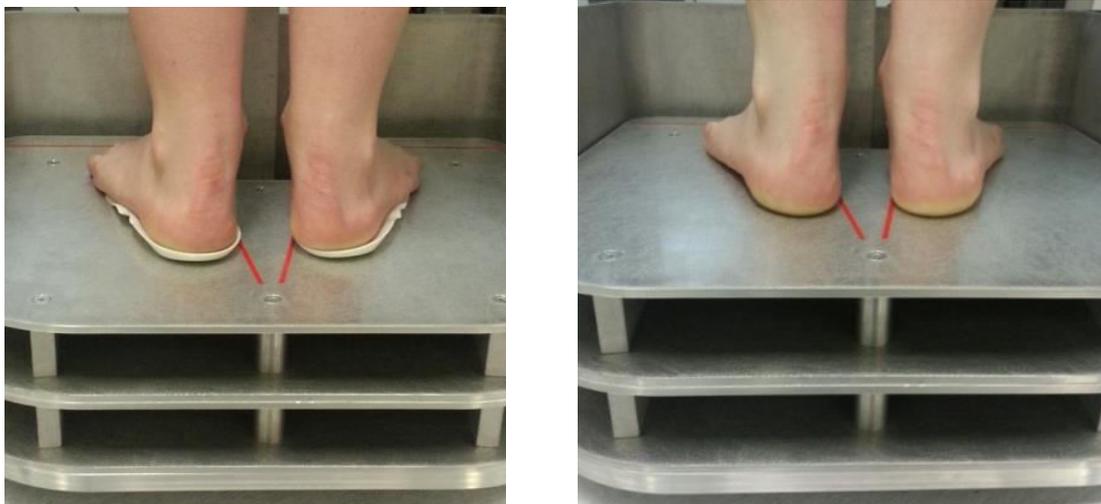
Figure 6. The left image shows the heel position of the subject while wearing insoles. The right image shows heel position of subject on scanner not wearing insoles. The heels, not the insoles, are aligned to the red line.
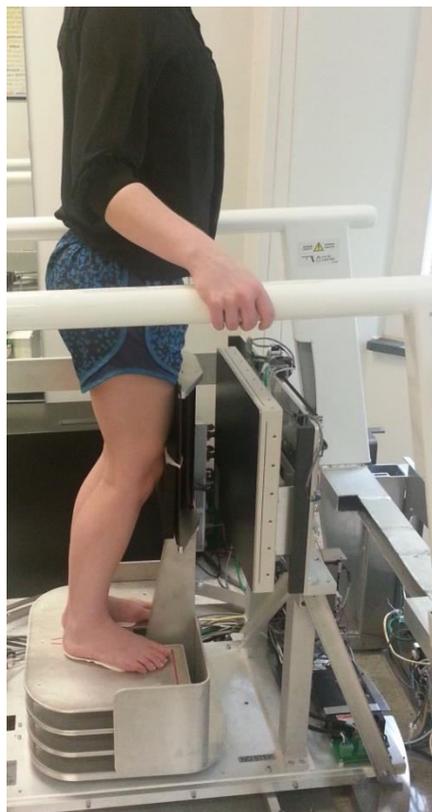
Figure 7. Subject position in weight-bearing CT scanner showing their knee, thigh, and elbow position.

Foot arch height was measured using an Arch Height Index Measurement System (AHIMS) in both sitting (non-weight-bearing) and standing (weight-bearing) positions, as seen below in Figure 8 (Jak Tool and Model, LLC, Matawan, NJ). The AHIMS is a reliable method of measuring arch height based on bony landmarks of the foot [65]. The measurements were obtained twice: once with the subject wearing the insoles, and once without the insoles. For the sitting measurements, the subject was seated on a chair with her hips and knees flexed at approximately 90 degrees and her feet resting on the floor. Each subject was asked to sit up straight and keep her hands on her lap and her weight evenly distributed between both feet. The standing measurements were conducted with the subject maintaining a comfortable stance with her feet shoulder-width apart, weight evenly distributed between both feet, and hands at her sides.

For each measurement, the heel cup of the AIHMS was placed firmly against the subject's heel and a horizontal sliding caliper was slid forward until it touched the most prominent toes to obtain the foot length. A second horizontal caliper was positioned at 50% of the total foot length. A third integrated vertical caliper was positioned on the dorsum of each foot and this height was recorded as arch height. Two measurements were taken in each position and averaged. If the two measurements differed by more than 2 mm, a third set of measurements was taken. Arch height measurements were used to determine the amount of change in arch height between sitting and standing conditions. To calculate arch drop, the standing arch height was subtracted from the sitting arch height.

Figure 8. Arch Height Measurement Index for arch height measurement.

MR images were acquired with the knees in a non-weight-bearing position. To ensure accurate registration of the MRI data to CT data, the angle of knee flexion was similar during both scans. This was accomplished by placing a small towel under the knee. A goniometer was used to measure knee flexion angle while the subject was positioned in the weight-bearing CT scanner. The size of the towel was adjusted so that the flexion angle while the subject was positioned in the MRI scanner matched the flexion angle while the subject was positioned in the weight-bearing CT scanner.

3.3 Model Creation

Tibiofemoral MRI data were collected with a Siemens 3T TIM Trio MRI scanner. The protocol included a 3D water-excitation sagittal dual echo steady state (SAG DESS

WE) sequence with 1.0 mm slice thickness. The weight-bearing CT data were acquired using a 3D cone beam CT with a voxel resolution of .37x.37x.37. All weight-bearing CT scans were collected with a tube voltage of 120 kVp and tube current of 5 mA.

Subchondral bone surfaces, articular cartilage, and menisci were manually segmented from sagittal MRI data using an interactive pen display and Osirix software (The OsiriX Foundation, Geneva, Switzerland). The segmentations were output in point cloud format and converted to .ply files. The .ply files were then exported for surface model creation in Geomagic Studio Software (Geomagic Studio Inc., Research Triangle Park, NC). Geomagic Studio allows the transformation of 3D scan data and polygon meshes into surface models. Each point cloud was loaded and wrapped using .3 mm point spacing. Geomagic Studio's hole filling algorithm was used to repair any gaps in the bone models. All holes on the bone models were filled except for those at the distal and proximal ends of the tibia and femur, respectively. After all bone, cartilage, and menisci models were wrapped and filled, they were refined and smoothed. Tibia and femur models were decimated to 16,000 facets, cartilage models were decimated to 5,000 facets, and menisci models were decimated to 4,000 facets. Each model was saved as a binary STL file for use in alignment and contact stress computation.

Subchondral bone surfaces were segmented from CT data using a semi-automated segmentation code. These bone models were exported to ITK-Snap and holes on the shaft of the bone models were manually filled. Each model was saved as a binary STL file for use in alignment.

3.4 Model Alignment and Registration

The subchondral bone surfaces from the MRI data were registered to the corresponding bone surfaces created with the weight-bearing CT data. The weight-bearing CT data allow for a subject-specific alignment to a functional loading. Femur models were loaded to the radiographic scene with the origin of the model corresponding to the origin of the scene. The alignment optimization was set up such that the femur could not travel past the film. Tibia models were aligned following the femur alignment by using the femur alignment transformation as an initial starting point. The outlined edges of the modeled bones were matched to the surface boundaries in the CT radiographs. Each alignment was visually assessed to confirm accurate alignment. MRI to CT registration was performed for both insole-supported and unsupported knees.

3.5 Tibial Rotation

Bone models for tibial rotation alignment were created through CT registration and through MRI to CT registration. Though the weight-bearing CT data and MRI data provide images of the knee, neither includes a full tibia. The portion of tibia viewed with MRI data is smaller than the portion of tibia obtained from weight-bearing CT data. Since the weight-bearing CT data provided the greatest length of tibia, models created through CT registration were used to develop a long axis, or principal axis, through the center of the bone shaft. The tibia rotates about this axis during internal and external rotation. The MRI to CT registered bone models were used to align the bone models once the principal axis was generated. Since these bone models consisted of the same bone, they would provide a precise alignment.

3.5.1 Principal Axis Creation

A principal axis was generated through the bone shaft of the tibia to observe

internal and external rotation of the tibial between insole-supported and unsupported

conditions. A standard joint coordinate system was constructed with an axis for

measuring internal and external rotation of the tibia. This axis was defined so as to pass

from the center of the tibial spine to the center of the most distal part of the tibia [66].

Because the weight-bearing CT scanner did not capture the full tibia, a 3D CAD tibia

model was used to computationally determine ideal positioning of the principal axis

(Figure 9) [67]. With the full tibia model, a principal axis was created to connect the

center of the tibial spine to the center of the distal tibia where it connects with the ankle.

Then, the tibia was shortened to 25% and 12.5% of its total length to observe changes in

position of the axis along the length of the tibia. At 25% of the total tibia length, the axis

was still positioned at the center of the most distal tibia. However, at the shortest length

(12.5% of full tibia length), the distal axis was observed to have shifted from the center

by about 20% in the posterior direction. Figure 10 shows the placement of the principal

axis on the distal tibia that is 12.5% the total length of the tibia. The average length of a

female tibia is approximately 365 mm [68]. Based on the available portion of the tibia

from the weight-bearing CT scans, the length of tibia used to determine tibial rotation in

each knee for this study was 12.5% of the total tibia length, or approximately 46 mm. All

tibia models longer than this length were trimmed in Geomagic Studio.
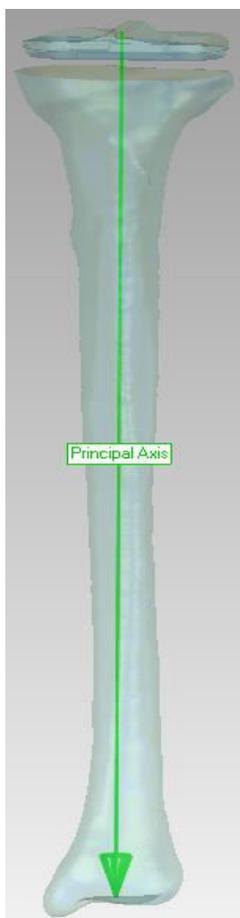
Figure 9. Full tibia model showing placement of principal axis.
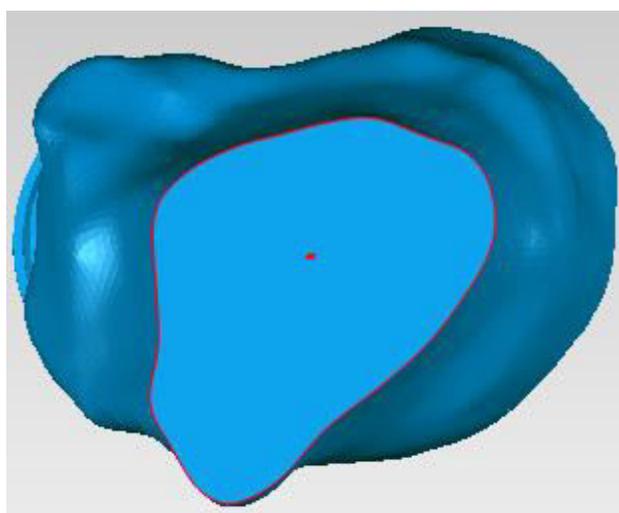
Figure 10. Position of principal axis at 12.5% of length of full tibia.

In each subject, the center of the most distal tibia was approximated in Geomagic Studio by selecting points along the peripheral border of the distal tibia and having the software compute the center position of a best-fit circle connecting those points. The anterior-posterior distance of the distal end of the tibia was calculated in Geomagic, and then the center point was shifted to a point approximately 20% posterior to the center.

Once the principal axis was created for each knee, a local coordinate system was generated using the principal axis as the longitudinal axis. The coordinate system was created on the unsupported tibia model and aligned with the longitudinal axis first (Figure 11). This coordinate system was then positioned in the center of the intercondylar eminence (Figure 12) [66]. The anterior-posterior (AP) axis was directed anteriorly for both right and left knees. The mediolateral (ML) axis was directed medially for left knees and laterally for right knees. The local coordinate system was set as the main coordinate system so that all translation and rotation for any bones would occur about this axis.
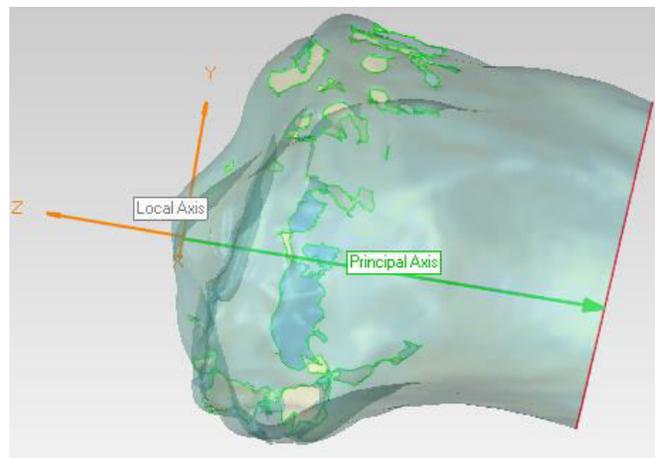
Figure 11. Local coordinate system is aligned with longitudinal axis (principal axis).
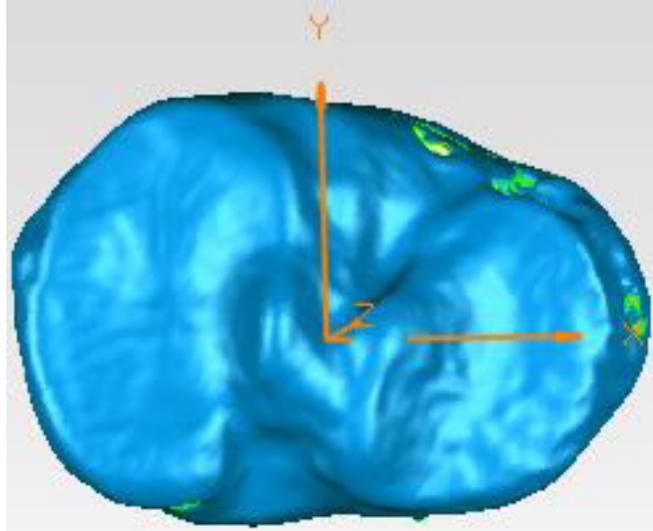
Figure 12. Placement of the local coordinate system at proximal tibia.

3.5.2 Model Alignment

The bone models that were generated via registration of MRI to CT data were

aligned with bone models registered from the CT data. Since the local axis had been

created based on the position of the CT generated bone models, the MRI bone models

were relocated into the same transformation matrix as the CT generated bone models.

After each MRI bone model was aligned to its corresponding CT bone model, the CT

bone models were removed from the Geomagic workspace. The transformation matrix

was cleared for each MRI bone model so that their transformed position became their

home position.

To determine tibial rotation between insole-supported and unsupported tibia

models, the insole-supported and unsupported knee models needed to be shifted into the

same position in space. To do that, the unsupported femur model was aligned with the

femur of the supported model. This was done using the registration function in Geomagic

to automatically align the two bones in the position that allowed the greatest overlapping

position. The amount of translation and rotation in all three planes for the unsupported

femur was recorded and applied to the unsupported tibia. At this point, the bone models

for both the supported and unsupported conditions are in the same position in space. An

overview of this process can be seen in Figure 13. Finally, the insole-supported tibia was

aligned to the unsupported tibia and the change in translation and rotation was recorded.
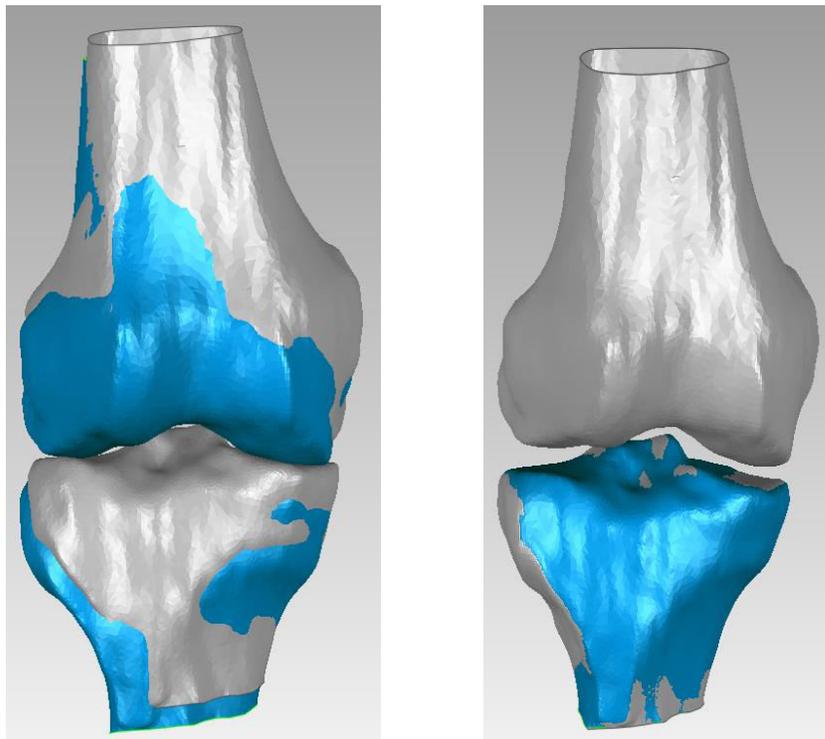
Figure 13. The left image shows the insole-supported and unsupported femur and tibia in the same transformation matrix. The right image shows the models with the unsupported femur aligned to the insole-supported femur and the unsupported tibia moved the same amount as the unsupported femur.

Since all the other conditions had been stabilized and held constant, the difference

in translation and rotation of the unsupported and supported tibia could be determined.

Positive rotation about the longitudinal axis for the supported tibia to align with the

unsupported tibia coincided to internal tibial rotation of the unsupported tibia for the right

knee. Negative rotation about the longitudinal axis for the supported tibia to align with

the unsupported tibia corresponded to internal tibial rotation of the unsupported tibia for

the left knee. Positive translation in the transverse plane was determined to be superior

movement for the right and left knees. Positive rotation about the ML axis for both the

left and right knee coincided with knee flexion. Positive translation in the sagittal plane

was determined to be lateral movement for the right knee and medial movement for the

left knee. Positive rotation about the AP axis was determined to be valgus condition for

the right knee and varus condition for the left knee, and positive movement in the coronal

plane corresponded with anterior movement for both the right and left knee.

<div align="center">3.6 DEA Implementation</div>

The DEA algorithm is implemented in MATLAB. DEA involves MRI

segmentation, refinement of the MRI segmentations to create surface models, and

alignment of the MRI segmentations to weight-bearing CT images. The bones were run

using displacement control DEA. With displacement control, joint load was not based on

body weight and varied for each knee and between insole-supported and unsupported

conditions. To run the DEA model with displacements, the bone models must first be

placed in the loaded position. Then closest-point pairings are made between the

articulating surfaces. Surface element pairings with proximities less than that of the

combined cartilage layer thickness are identified, and all further calculations are

computed on only these elements. Individual deformations of the springs are computed as

the difference between their proximity and the cartilage thickness. Contact stress (p) is

calculated from this deformation with a force-displacement spring model. This model

uses the spring stiffness multiplied by spring deformation (d). The spring stiffness is a function of Young's Modulus (E), Poisson's ratio (v), combined cartilage thickness (h) [8, 49]. The values of Young's Modulus used were 4 MPa for cartilage and 20 MPa for meniscus. 0.42 (cartilage) and 0.30 (meniscus) were the values of Poisson' ratio used.

$$p = \frac{E\,(1\text{-}v)\,d}{(1\text{+}v)(1\text{-}2v)\,h}$$

The implemented DEA algorithm consists of two rigid contact surfaces lined with a system of linear springs as contact points. The algorithm computes contact stress at a particular joint position. The resulting reaction forces are computed and the solution is checked against completion of termination constraints. Iterations continue until the termination constraints of the simulation have been met.

For each iteration, an assumption is made that no contact exists between the surfaces and there are no springs connected to the surfaces. Every iteration begins by selecting the nearest neighbor between polygon centroids on contacting surfaces. Next, a system of springs is created between the nearest neighbors and a displacement is applied. Overlap is determined by contacting surfaces and a system of springs is created between the contacting regions. The deformation of each spring is computed and then related to the contact stress on the contact surface.

Adjacent polygons on two opposing surfaces are used to accurately detect contact between two surfaces. The spring models used in this algorithm assume that the stresses on each polygon are normal to the face of the polygon. Cartilage thickness varied for each knee based on manual segmentation of the cartilage from the MRI data. The contact pressures and areas for each contacting polygon are used to compute the discrete contact

forces acting on the contact surfaces. The process from segmentation to DEA implementation is summarized below in Figure 14.

Contact stress is computed for each facet on the contact region. Results for each knee were loaded and displayed onscreen in the form of a contact stress distribution. Using mouse selection in MATLAB, the medial and lateral compartments of each knee were separated. Following this separation, mean and maximum contact stresses were recorded for both the medial and lateral compartments. Using DEA results, the area of contact stress on the medial and lateral compartments was plotted.

A hindrance to using displacement control DEA is that all contact is very sensitive to even small changes in displacement. An alternative method of computing contact stress is through load control. Load control involves application of a standard load to each knee. However, the change in position of the menisci was to be observed in the DEA results, so displacement control was chosen in this case.
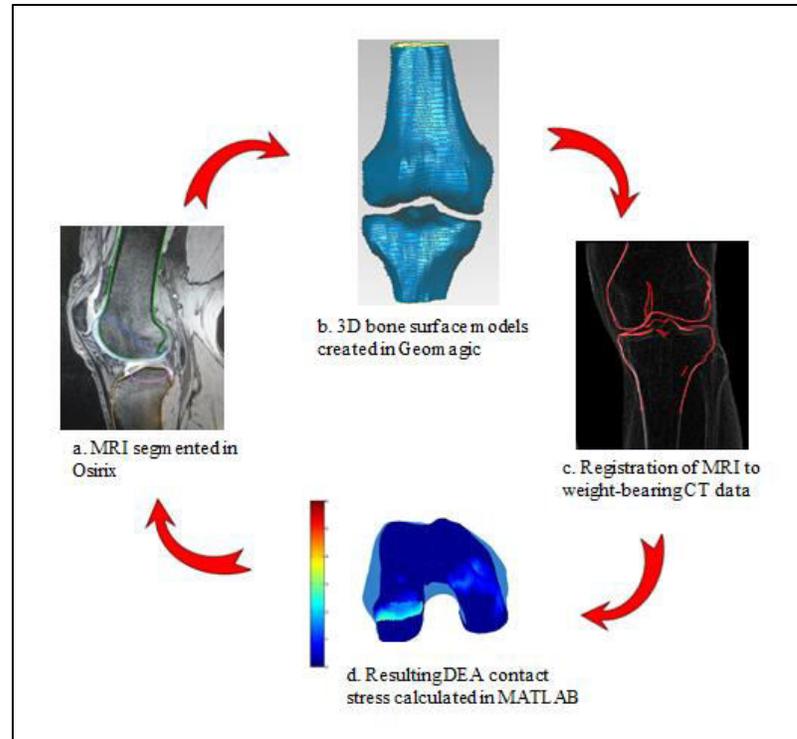
Figure 14. DEA implementation process. The method begins with segmentation of subchondral bone from MRI scans. From these scans, 3D bone surface bones are generated and registered to weight-bearing CT data for insole-supported and unsupported knees. The DEA algorithm is used to compute a contact stress evaluation and the resulting calculations are plotted in MATLAB.

CHAPTER 4: RESULTS

4.1 Arch Height Measurements

For all subjects, a mean drop in arch height of approximately 4.3 mm with a standard deviation of 3.18 mm was observed between insole-supported and unsupported conditions. Arch height measurements indicate a change in arch height between sitting and standing positions for both insole-supported and unsupported conditions. Despite the similar arch drop values, the magnitude of the arch height changed between insole-supported and unsupported conditions, with mean arch height values being larger for insole-supported feet. Figure 15 shows the difference in arch height for insole-supported and unsupported feet.
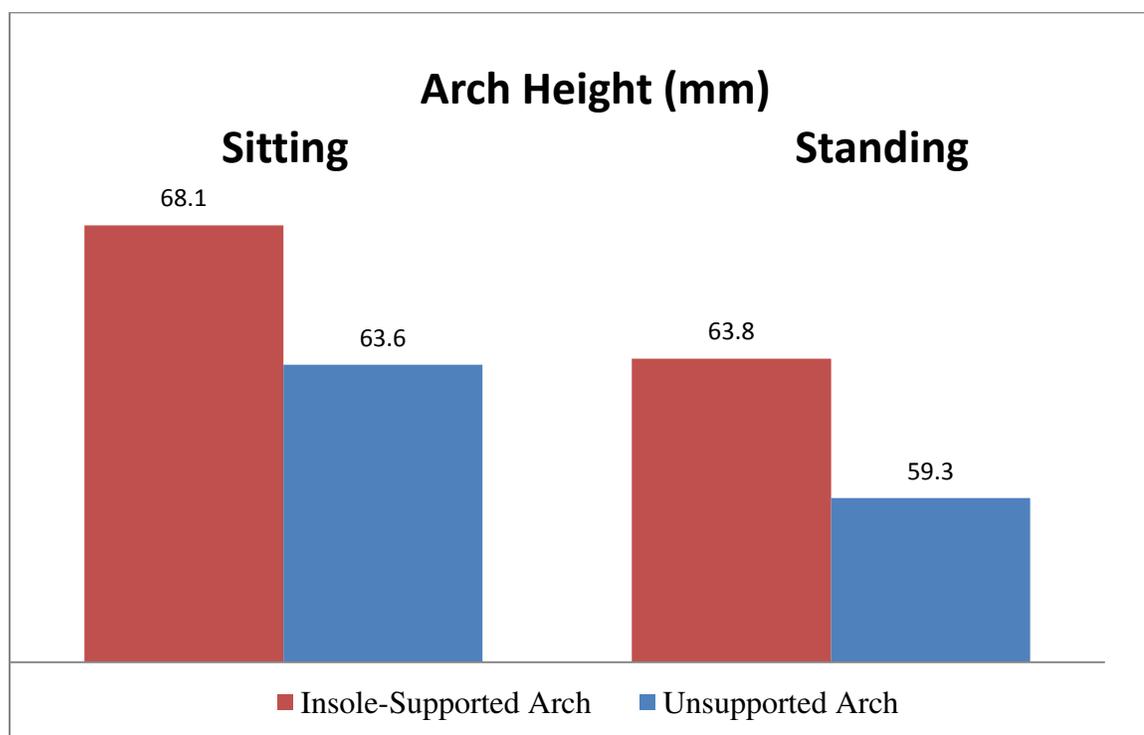
Figure 15. Arch height data for sitting and standing position for both insole-supported and unsupported conditions.

4.2 Tibial Rotation

All absolute tibial rotation and translation values in each Cartesian direction can be found in Table 1. The mean absolute value of tibial rotation about the z-axis (longitudinal axis) of unsupported knees compared to insole-supported was found to be 1.02°±1.13°. While the majority of knees had a change in tibial rotation about the longitudinal axis of less than 1 degree, three knees showed no substantial change in rotation of the tibia along the principal axis between insole-supported and unsupported conditions.

Net tibial rotation and translation values in each Cartesian direction can be found in Table 2. The mean value of tibial rotation about the longitudinal axis in the unsupported condition compared to the insole-supported condition was found to be 0.75°±1.33° of internal rotation. A p-value of 0.009 was obtained for a one-tailed one-sample t-test, indicating that there is a statistically significant difference in tibial rotation for the arch-unsupported condition when compared to the arch-supported condition. Figure 16 shows the direction and magnitude of tibial rotation for each knee.

In addition to rotation about the longitudinal axis, movement of the tibia was observed along each axis and rotation was observed along both the ML axis and AP axis. The largest magnitude of translational change in position was seen in the coronal plane. There was also measurable translation in the sagittal and transverse planes. There was measureable rotation about the ML axis and AP axis, in addition to rotation about the longitudinal axis. The smallest rotational change in tibial position was observed about the AP axis, and the largest rotational change was observed about the ML axis.

Table 1. Tibial Rotation and Translation Values for all Unsupported Arch Conditions
Compared to Arch-supported Conditions.

Knee Number	ML Translation (mm)	AP Translation (mm)	Longitudinal Translation (mm)	ML Rotation (degree)	AP Rotation (degree)	Longitudinal Rotation (degree)
1	0.62	5.98	1.62	2.93	0.20	0.22
2	0.33	3.15	0.98	1.31	0.20	0.20
3	0.25	4.86	1.73	1.86	1.10	2.56
4	0.95	0.42	0.39	0.53	0.27	1.68
5	0.76	3.22	2.29	2.92	1.12	0.17
6	1.02	5.39	1.76	4.76	1.07	0.23
7	0.35	2.30	0.90	0.94	0.11	0.01
8	0.18	1.38	0.64	0.81	0.20	0.25
9	2.29	9.00	2.20	3.21	0.13	2.50
10	1.13	0.08	0.42	0.30	0.78	0.25
11	0.42	1.45	0.26	0.22	0.09	1.06
12	0.41	1.61	0.75	1.21	0.30	0.49
13	0.48	2.36	0.52	0.50	0.36	0.80
14	1.18	4.02	0.97	1.10	0.80	3.82
15	0.10	1.75	0.61	1.52	0.32	0.78
16	1.72	7.39	1.82	3.26	0.22	2.89
17	0.69	2.64	1.45	1.97	0.35	1.24
18	1.01	5.25	2.69	3.76	0.54	0.03
19	0.12	4.74	2.12	4.15	0.49	2.06
20	1.15	1.57	0.93	0.92	0.62	0.04
21	0.92	1.67	0.04	0.97	0.87	0.13
Mean	0.77	3.34	1.19	1.86	0.48	1.02
Standard Deviation	0.56	2.33	0.76	1.36	0.34	1.13

Table 2. Magnitude and Direction of Tibial Rotation and Translation Values for
Unsupported Arch Conditions Compared to Arch-supported Conditions.

	ML Translation (mm)	AP Translation (mm)	Longitudinal Translation (mm)	ML Rotation (degree)	AP Rotation (degree)	Longitudinal Rotation (degree)
Mean	0.49 Lateral	0.50 Anterior	-0.15 Superior	0.102 Extension	0.186 Valgus	0.75 Internal
Standard Deviation	0.82	4.11	1.43	2.34	0.57	1.33
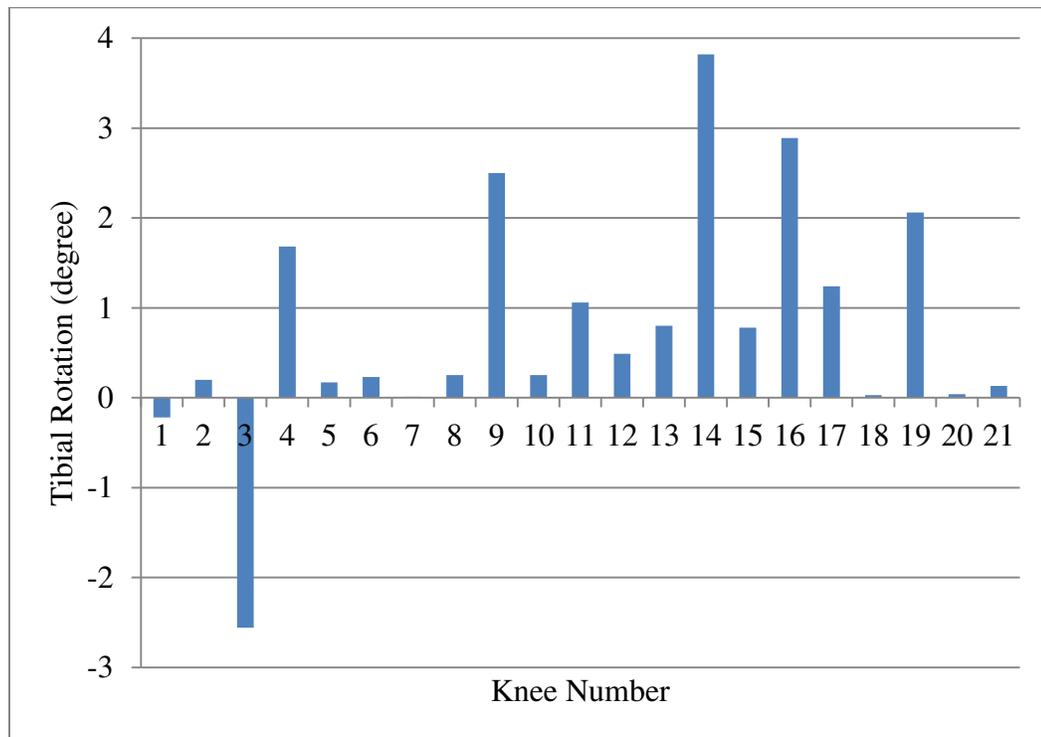
Figure 16. Direction and Magnitude of Change in Tibial Rotation. Internal rotation is
depicted as positive rotation, and external rotation is depicted as negative rotation.

4.3 Contact Stress Results

The DEA contact stress method was used to evaluate contact stress between the

cartilage surfaces of 21 knee models. Contact stress for insole-supported and unsupported

knees is depicted in Figures 17 and 18, respectively. These contour plots reflect contact

stress magnitude and distribution for insole-supported and unsupported knees. Cooler colors indicate lower DEA contact stress computation, while warmer colors indicate higher DEA contact stress computation. The majority of contact stresses on all knees were small in magnitude. This outcome was expected because all subjects had healthy knees. Larger stress values were mainly present on the borders of contact for the meniscus and cartilage, or areas of high incongruity. The effect of the meniscus on contact stress placement is shown in Figure 19. From this image, it is perceived that the meniscus plays a role in contact stress displacement because the majority of contact stress is located at the articulation point of the meniscus and cartilage.
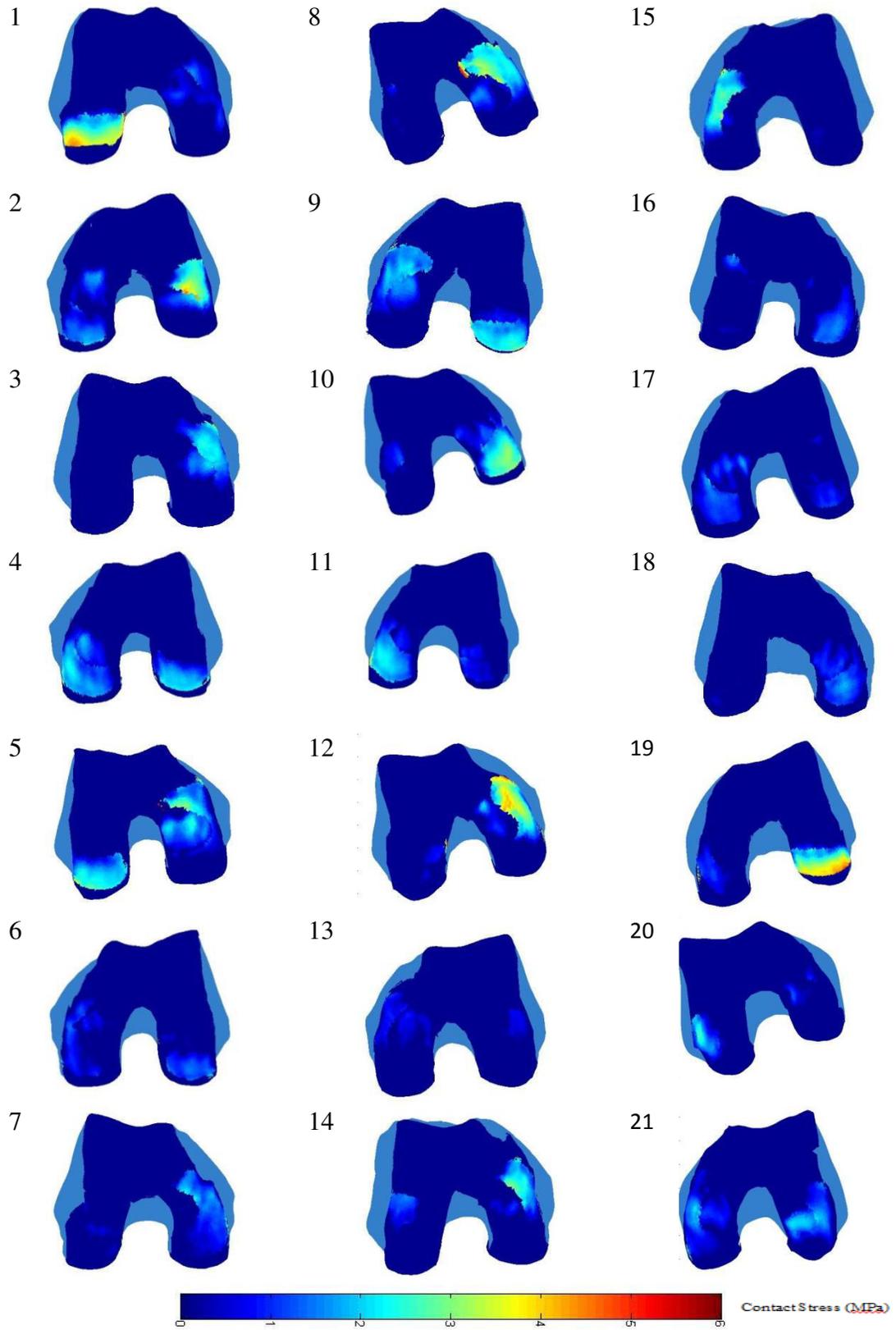
Figure 17. Contact stress magnitude and distribution for insole-supported knees.
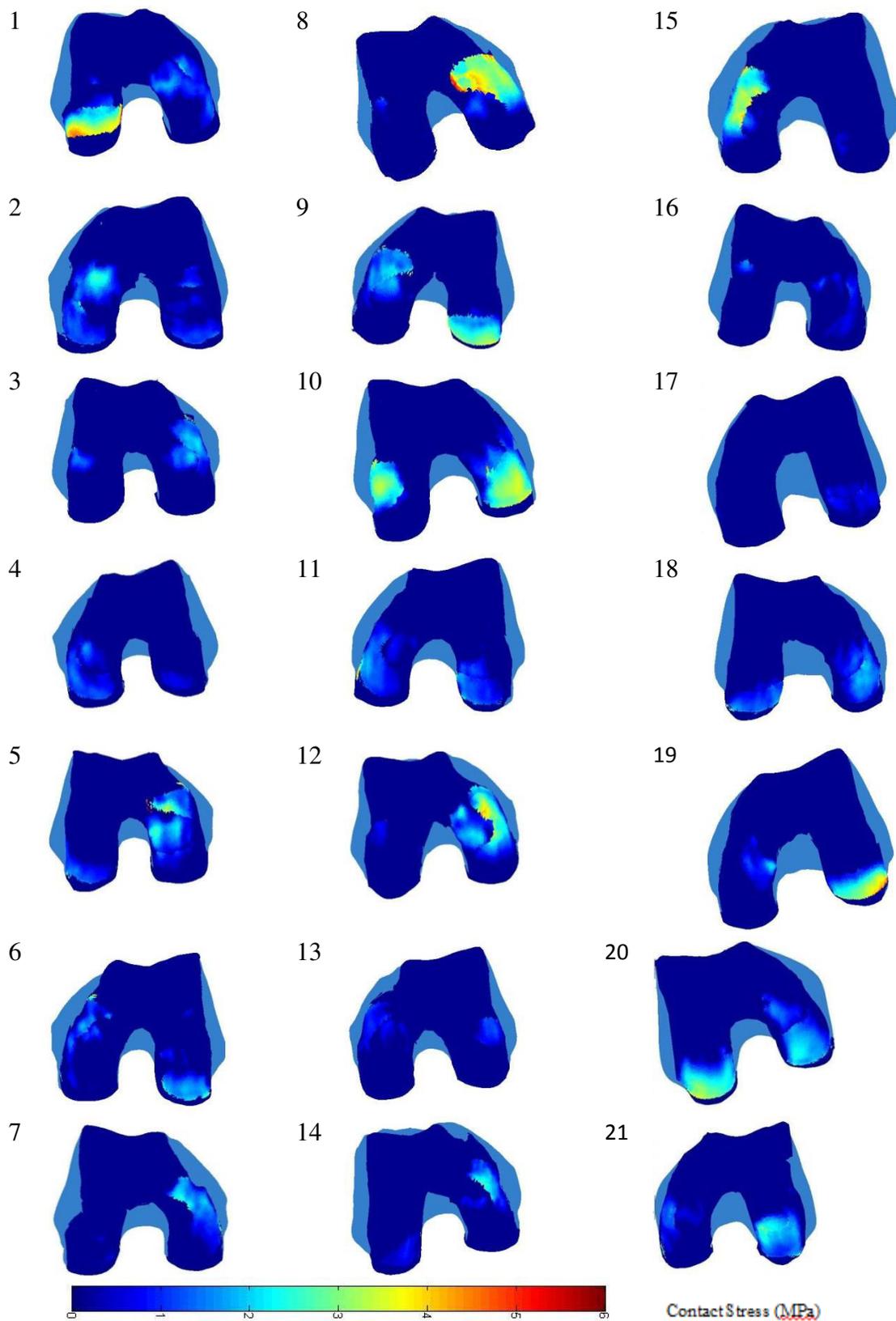
Figure 18. Contact stress magnitude and distribution for unsupported knees.
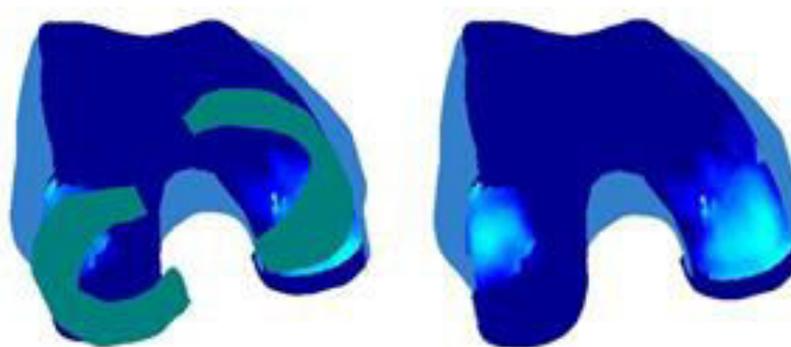
Figure 19. The left image shows the placement of the meniscus on an insole-supported knee. The right image shows contact stress on the same knee with the meniscus removed.

Table A-2 shows mean contact stress for both medial and lateral compartments in insole-supported and unsupported knees. As seen below in Figure 20, there was no substantial change in mean contact stress within each side for either condition. However, the mean contact stress on the lateral compartment was approximately 15% smaller than the mean contact stress on the medial compartment for both conditions. The results of a one-tailed paired t-test indicate that there were no differences comparing the mean contact stress for either the lateral and medial compartments, comparing the arch-supported with the arch-unsupported conditions ($p=0.41$ for lateral; $p=0.45$ for medial).

The magnitudes of maximum contact stress for both the medial and lateral compartments for insole-supported and unsupported conditions can be seen in Table A-3. Unsupported knees had similar maximum contact stress values for both the medial and lateral sides (Figure 21). The majority of the maximum contact stress was located along the edge of meniscus and cartilage contact. There were no differences comparing the maximum contact stress for either the lateral and medial compartments, comparing the

arch-supported with the arch-unsupported conditions (p=0.23 for lateral; p=0.06 for

medial).
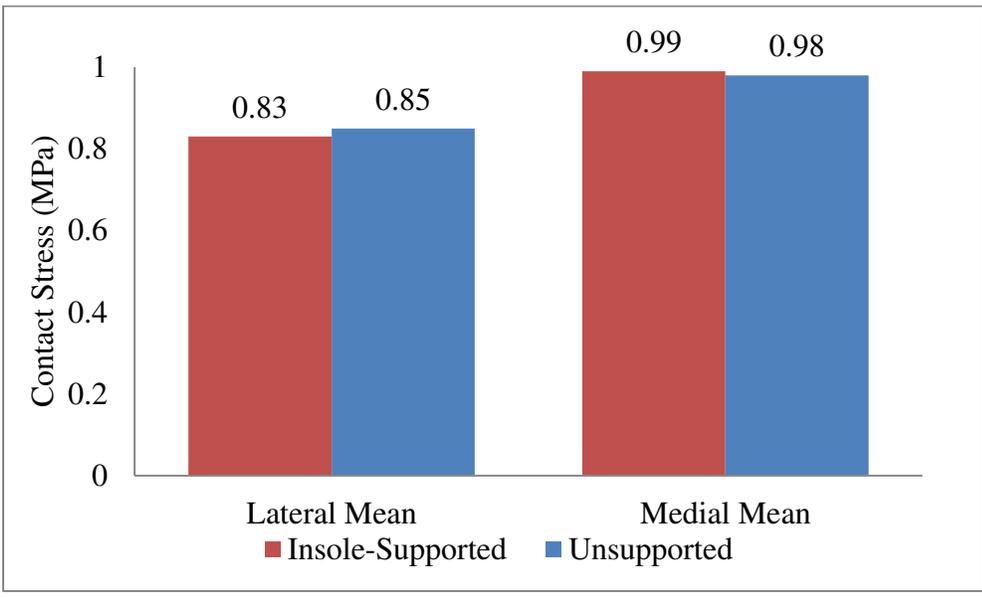
Figure 20. Relationship between Mean Contact Stress for Unsupported and Insole-Supported Conditions.
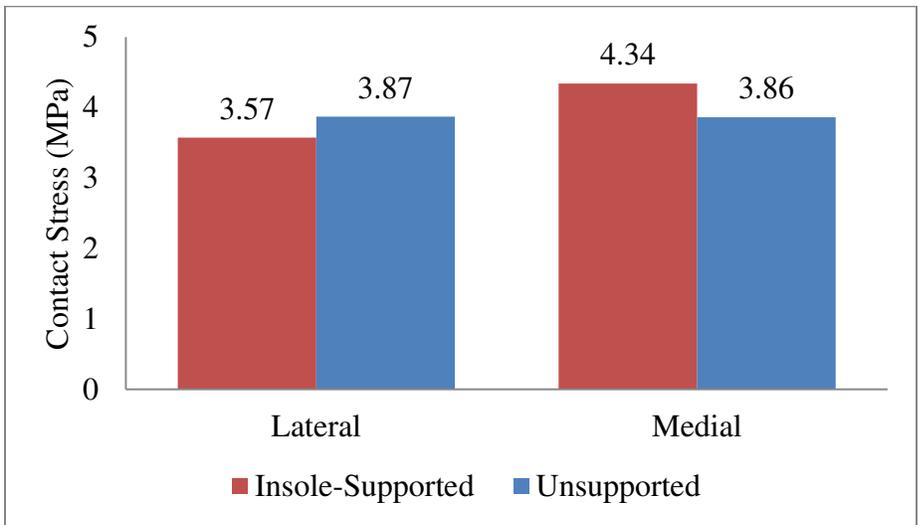
Figure 21. Relationship between Maximum Contact Stress for Unsupported and Insole-Supported Conditions.

4.3.1 Contact Area

Contact areas were compared for insole-supported and unsupported knees. The mean contact area for the lateral compartment was found to be 13% larger in unsupported conditions. For the medial compartment, there was no significant difference in mean contact area in insole-supported and unsupported conditions. The relationship between contact areas for both the medial and lateral sides for insole-supported and unsupported knees is depicted below in Figure 22. There were no differences comparing the contact area for either the lateral and medial compartments, comparing the arch-supported with the arch-unsupported conditions with a one-tailed paired t-test (p=0.13 for lateral; p=0.44 for medial).
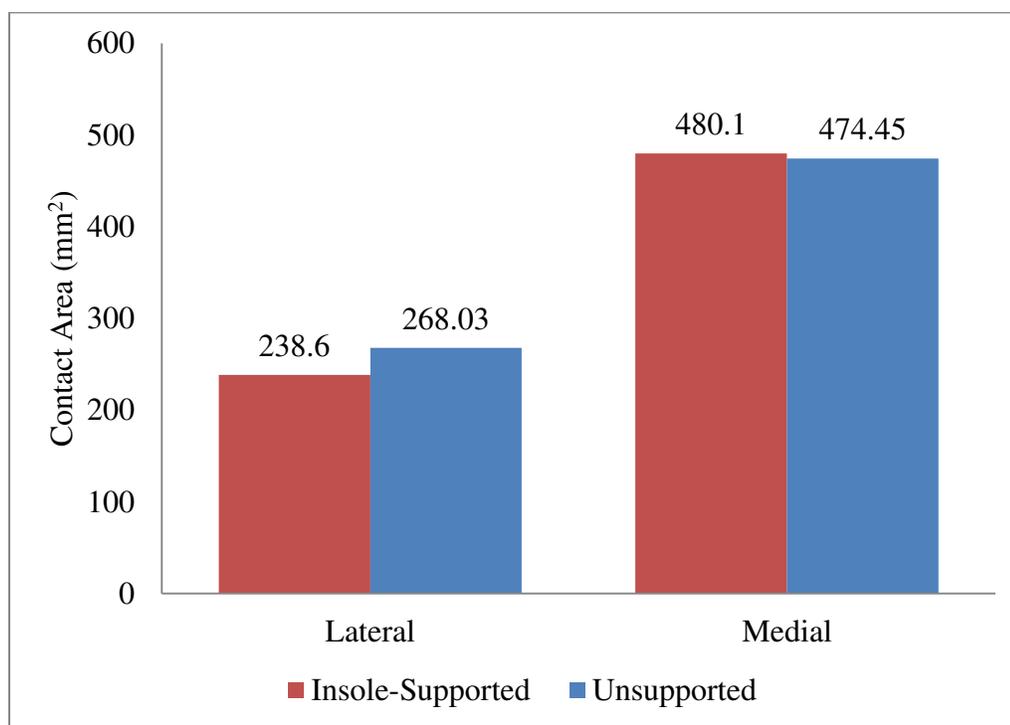
Figure 22. Difference in contact area of lateral and medial compartments for insole-supported and unsupported knees.

A larger contact area on the medial compartment indicates that stress was more wide-ranging on the medial side in insole-supported cases compared to unsupported. The difference in mean contact area on the medial and lateral sides was expected due to the effect of the arch support. When the arch height is increased from a flat arch to a more normal arch height, it is expected that the tibia will shift to a more neutral position, changing the contact area on each compartment of the knee.

4.3.2 Joint Force

A measureable difference in joint load was observed between insole-supported and unsupported knees. The unsupported knees had a smaller mean joint load compared to the insole-supported knees. Figure 23 shows the differences observed in applied load for each knee. The magnitude of force in each knee model can be seen in Table B-1. Joint force is dependent on knee position and subject weight, so it varied from subject to subject. The mean joint load was 742.9 N for insole-supported knees and 773 N for unsupported knees. On average, joint load was approximately equal to body weight for insole-supported knees and approximately 1.1 times body weight for unsupported knees.

The change in joint load as a percentage of total body weight was compared for arch-supported and unsupported conditions (Figure 23). The mean difference in joint force between unsupported conditions and insole-supported conditions was found to be approximately 30.5 N. There was no difference comparing the joint load for the arch-supported with the arch-unsupported conditions (p=0.35).
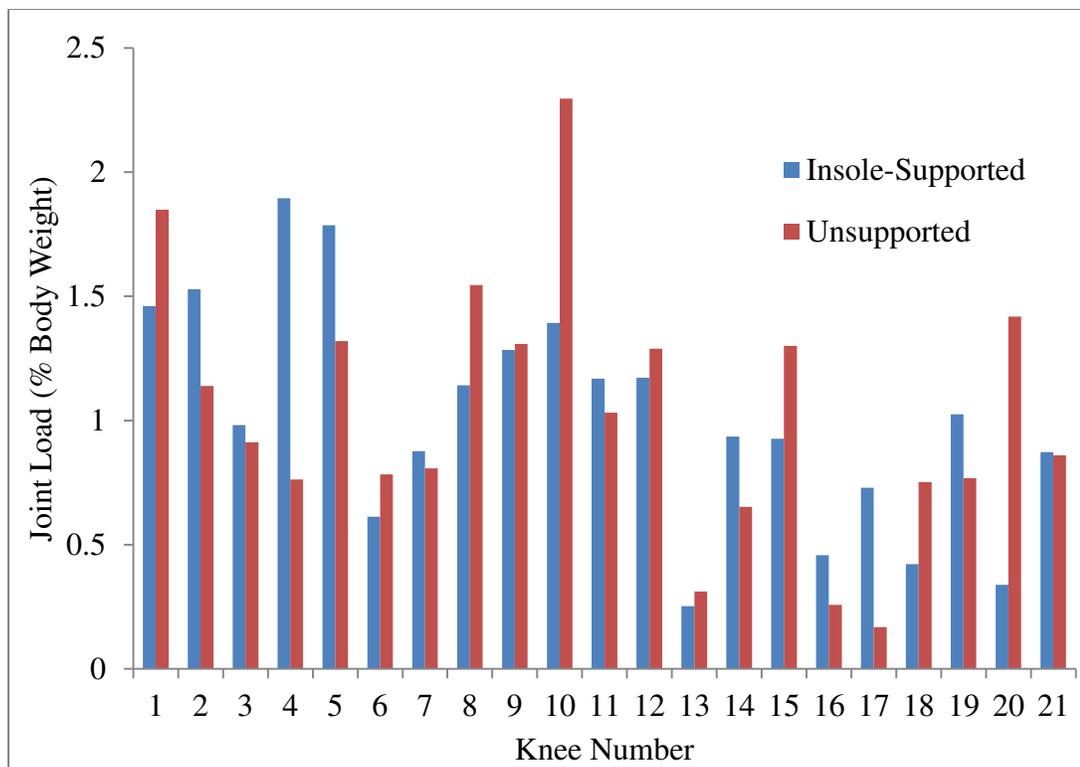
Figure 23. Difference in joint load for insole-supported and unsupported conditions.

CHAPTER 5: CONCLUSION

5.1 Discussion of Results

Compared to insole-supported knees, knees with unsupported arch height had a mean tibial rotation of approximately 1.02° about the longitudinal axis. It was also observed that there was a change in tibial translation and rotation in all directions when the arch height was not supported. Changes in position of the tibia were expected due to the presence of the arch support.

Three knee models did not have a measurable change in tibial rotation between insole-supported and unsupported conditions. This outcome is likely a result of the subject altering their foot position during their second weight-bearing CT scan so that their toes were positioned laterally to their ankle, thereby negating the effect of the arch supports on change of tibial rotation. The subject may have also kept their foot in a tensed position after the removal of the arch insole, preventing their calcaneus and tibia from rotating naturally.

There was a measureable shift of the tibia along the ML axis of an average of 0.77 mm for unsupported knees compared to insole-supported knees. This may indicate signs of IBFS. Due to iliotibial band friction syndrome, tightness and shortness of the iliotibial band may force both the tibia and patella to shift laterally. Lateral tibial translation may also be due to ligamentous laxity. Internal tibial rotation may over-stretch supporting cruciate ligaments, effectively decreasing their ability to constrain tibial movements [38, 39].

Mean tibial translation along the AP axis of approximately 3.34 mm was observed in unsupported knees. This was the greatest shift in positioning of the tibia observed in

any direction. As seen above in Table 2, the direction of the net change along the AP axis was found to be anterior. Anterior tibial translation is caused by internal tibial translation because the strength of the anterior cruciate ligament is hindered by the internal rotation of the tibia. ACL strength is hindered because tibial rotation will cause the ligament to stretch and may reduce its laxity. This is the main ligament that prevents translation in the anterior direction, so its laxity enables anterior translation of the tibia [43]. This translation may also be due to internal rotation pulling the lateral tibial condyle anteriorly.

In addition to tibial rotation, there was noticeable rotation about the ML axis in the sagittal plane of an average of approximately 1.86 degrees for unsupported knees in comparison to insole-supported knees. This rotation indicates knee flexion or extension. This was expected because the arch insole would decrease the distance between the ankle and the knee joint by raising the arch height. Removal of the arch insole would increase distance between the two joints, causing the knee to extend so that the feet can rest on the ground.

Rotation about the AP axis (in the coronal plane) produced the smallest change in position of the tibia (.48 degrees). Foot pronation may lead to development of a valgus condition by causing the distal femur and proximal tibia to shift medially. This movement, combined with no change in position of the hip, may occur when the tibia is rotated internally. This leads the tibia and femur to articulate more closely on the lateral side rather than the medial side [36]. Foot pronation and subsequent internal tibial rotation cause lateral superior translation of the tibia to accommodate the inward shift of the bones.

Contact stress is understood to play a significant role in many aspects of joint degradation. DEA is a useful technique for the investigation of the effects of arch height on tibiofemoral contact stress using a simplified computational methodology. Due to the change in position of the tibia due to the arch insole, it is expected that contact stress will be altered because of the altered alignment of the tibia and femur.

Figures 17 and 18 show changes in contact stress magnitude and distribution for all knees between insole-supported and unsupported conditions. The change in tibial position causes malalignment of the knee joint, leading to differences in contact stress area depending on the movement of the tibia. Some of the knees had increased contact stress values located near the edge of the cartilage and bone. This is due to displacement of the meniscus, which is considered to not move with respect to the tibia. The meniscus absorbs much of the force in the knee and shifts positions based on rotation of the tibia. Previous work involving DEA methods on a knee model which included meniscus showed that the meniscus mainly impacts contact stress around the peripheral tibial plateau but regions of peak contact stress near the center of the tibial plateau are relatively unaffected by the meniscus [8]. The presence of a meniscus in the knee model is thought to increase the contact area of normal knees. A previous study found a mean lateral contact area of 420 mm^2 and a mean medial contact area of 530 mm^2 for healthy knee models with a meniscus included and an applied joint load of approximately 112lb [69]. The values of contact areas obtained with DEA for this study are consistent with values obtained for normal knees in this previous study.

There was a change in contact area between the medial and lateral sides for supported and unsupported conditions. Contact areas for each knee can be seen in Table

A-1. Though contact area on the medial compartment remained fairly constant for both insole-supported and unsupported conditions, the mean contact area of the lateral compartment was 11% greater for unsupported knees in comparison to insole-supported knees. On average, the contact area on the medial compartment was approximately 50% greater than the contact area on the lateral compartment, which is consistent with findings of previous studies [70, 71]. The change in contact area is consistent with a shift in knee alignment from normal to valgus. Mean contact area for knees that exhibit knee osteoarthritis characteristics has been found to be approximately 1220 mm^2 [55]. The mean contact area for insole-supported knees and unsupported knees was found to be 718 mm^2 and 742 mm^2, respectively, in this study. Since the recruited subjects had healthy knees, the contact area is expected to be smaller than that of knees that are showing signs of degeneration.

Mean contact stress on the medial compartment was approximately the same for both insole-supported and unsupported conditions. The mean contact stress on the lateral compartment was approximately 15% smaller than the mean contact stress on the medial compartment. The arch insole caused approximately a 12% increase in the maximum medial contact stress, and an 8% decrease in the maximum lateral contact stress.

The amount of force applied on each knee varied based on the subject's weight. Due to the change in foot position and subsequent spread of shock absorbed, the amount of force absorbed by the knee joint varies. This is partly due to changes in the alignment of the joint because of tibial rotation and translation, which may increase joint force in other lower extremity areas. An increase in joint force in unsupported knees may be due to increased muscle tension because of the position of the foot.

Contact stress exposure is thought to play a role in joint degradation. Effective contact stress computation in normal joints is vital in determining the role of contact stress in development and progression of knee osteoarthritis.

5.2 Potential Clinical Impact

The findings from this study may be used to predict future development of musculoskeletal disorders in the lower limbs. A drop in arch height indicates changes in tibial rotation and contact stress at the tibiofemoral joint. If physicians are able to attribute lower limb musculoskeletal disorders to problems that arise during pregnancy, they may prescribe women to wear orthotic insoles in their shoes throughout their pregnancy. This could potentially decrease the population of women who develop knee pain and knee osteoarthritis, as well as related musculoskeletal disorders. Preventing development of knee osteoarthritis or other lower limb musculoskeletal disorders could decrease joint disability and improve the quality of life for women.

5.3 Limitations

Several limitations exist for the current tibial rotation and DEA study. Since this was a preliminary study, a small sample size was chosen. Increasing the sample size for future studies may lead to more significant results.

Due to the cross-sectional design of this study, there was no way of knowing whether the lasting decrease in arch height was due only to pregnancy effects or whether there was a further drop in arch height that occurred after pregnancy. The change in arch height was simulated with the aid of orthotic insoles since the study was conducted longitudinally with respect to the pregnancy. Since it is possible for arch height to change due to other conditions, arch height measurements and weight-bearing CT scans should

be taken immediately before and after pregnancy to ensure that any change in arch is due to the effects of the pregnancy.

Another limitation was that the height of the arch insoles was not accounted for. The measured thickness of the insoles was approximately 4.5mm, which is equivalent to the change in arch height between unsupported and supported arch height. Therefore, it is possible that the insoles used in this study raised the position of the foot, rather than raise the arch height of the foot. This may explain why only small changes in tibial rotation and contact stress were found. In the future, thinner insoles may be used to ensure that there is a change in arch height.

5.4 Future Work

The current study evaluated the impact of an artificial change in arch height on tibial rotation and tibiofemoral contact stresses. Although the study was able to reveal insights into the effects of an arch insole, a more complete analysis is desired to determine the effects of arch drop due solely to pregnancy issues. The cross-sectional design of this study made it impossible to know whether subject's arch drop was caused by pregnancy effects only. Although implants were used to artificially adjust arch height, the minor changes in tibial rotation suggest that the study protocol needs to be reconstructed.

The current study focused solely on the movement of the tibia and assumed a steady position of the femur. Rotation at the hip joint may affect posture by altering the alignment of the femur and tibia, potentially leading to development of lower limb musculoskeletal disorders. Computational analysis of femoral rotation and translation

with respect to tibial rotation and translation may provide better understanding of the effect of arch height on tibiofemoral contact stress.

5.5 Summary Statement

The goal of this research was to investigate whether a drop in foot arch height leads to an increase in internal tibial rotation and medial tibiofemoral contact stress in postpartum women with flexible foot arches. The study results indicated that a decrease in arch height appeared to cause a small increase in internal tibial rotation about the longitudinal axis. No significant changes in medial or lateral tibiofemoral contact stress were found. Further analysis can be completed to test the effect of arch insoles on other lower limb musculoskeletal disorders.

APPENDIX A: CONTACT STRESS RESULTS

Table A-1. Contact Area for Insole-Supported and Unsupported Knees Using DEA.

Knee Number	Supported Lateral Contact Area (mm)	Supported Medial Contact Area (mm)	Unsupported Lateral Contact Area (mm)	Unsupported Medial Contact Area (mm)
1	440.9	431.5	474.6	621.9
2	436.4	550.3	429.7	674.2
3	0.000	478.0	109.5	436.4
4	355.5	645.0	145.1	552.5
5	380.7	650.4	259.1	713.3
6	320.1	393.6	376.6	302.4
7	134.7	643.6	88.70	496.1
8	79.50	685.8	67.90	676.0
9	549.7	540.9	477.0	481.6
10	144.2	637.5	290.4	664.8
11	277.7	590.8	392.6	542.3
12	135.8	575.8	96.80	795.3
13	103.5	358.5	154.1	305.2
14	154.0	337.9	192.9	303.0
15	38.80	362.3	60.30	440.3
16	86.50	305.7	44.80	300.1
17	215.2	519.3	264.3	13.00
18	58.10	496.1	370.3	524.7
19	416.5	221.6	357.7	234.4
20	259.1	108.4	468.4	558.3
21	423.0	549.9	507.8	327.7

Table A-2. Mean Lateral and Medial Contact Stress for
Insole-Supported and Unsupported Knees Using DEA.

Knee Number	Insole-Supported		Unsupported	
	Lateral (MPa)	Medial (MPa)	Lateral (MPa)	Medial (MPa)
1	1.65	0.60	1.75	0.93
2	1.58	0.92	0.60	1.09
3	0.00	1.31	0.46	1.15
4	0.96	1.26	0.25	0.84
5	1.06	1.33	0.49	1.32
6	0.86	0.61	1.01	0.86
7	0.65	0.66	0.69	0.73
8	0.35	1.43	0.40	1.75
9	1.28	1.26	1.44	1.18
10	0.45	1.38	1.36	1.48
11	0.59	1.03	0.97	0.75
12	0.84	1.72	0.65	1.58
13	0.29	0.63	0.47	0.63
14	1.56	1.14	0.81	0.92
15	0.29	1.20	0.36	1.39
16	0.33	0.71	0.43	0.59
17	0.48	0.85	0.47	0.15
18	0.31	0.86	1.06	0.90
19	1.91	0.54	1.40	0.42
20	0.79	0.49	1.31	1.23
21	1.18	0.81	1.52	0.64

Table A-3. Maximum Lateral and Medial Contact Stress
Values for Insole-supported and Unsupported Knees
Using DEA.

Knee Number	Insole-Supported		Unsupported	
	Lateral (MPa)	Medial (MPa)	Lateral (MPa)	Medial (MPa)
1	5.20	1.66	6.16	2.25
2	5.00	2.64	2.47	2.92
3	0.00	4.14	3.46	4.01
4	4.86	4.69	2.90	2.88
5	4.36	6.38	3.54	5.85
6	6.20	4.47	6.50	3.85
7	4.97	3.42	4.19	3.60
8	3.21	5.32	3.01	5.57
9	5.09	3.95	4.95	3.92
10	1.54	3.53	3.40	4.45
11	2.93	4.49	4.53	4.24
12	7.14	5.33	4.19	4.91
13	0.75	3.42	1.37	3.05
14	6.06	7.80	7.88	8.06
15	0.47	5.27	0.66	5.13
16	2.70	5.48	1.95	5.19
17	1.18	3.81	1.06	0.50
18	2.88	1.82	5.78	2.16
19	5.31	4.49	5.46	2.14
20	2.92	1.28	4.33	2.78
21	2.16	7.65	3.49	3.49

APPENDIX B: KNEE JOINT FORCE

Table B-1. Knee Joint Force for Insole-Supported and
Unsupported Knees Using DEA.

Knee Number	Insole-Supported Knees Joint Load (N)	Unsupported Knees Joint Load (N)
1	1085.2	1374.1
2	1135.3	846.8
3	563.0	523.7
4	1087.3	437.3
5	1295.5	957.2
6	444.0	567.4
7	585.2	538.7
8	1030.9	1395.2
9	1159.3	1181.2
10	942.1	1552.8
11	790.5	697.5
12	1016.7	1118.3
13	219.6	270.1
14	524.4	365.8
15	519.0	728.9
16	305.3	171.7
17	486.2	111.9
18	396.5	705.8
19	962.4	720.4
20	294.2	1230.5
21	757.5	746.1

REFERENCES

1. National Center for Health Statistics. Health, United States, 2010: With Special Feature on Death and Dying. Hyattsville, MD. 2011. Web. Available: http://www.cdc.gov/nchs/data/hus/hus10.pdf. Accessed [06 01 2014].

2. "Osteoarthritis." *Centers for Disease Control and Prevention*. Centers for Disease Control and Prevention, 16 May 2014. Web. Available: http://www.cdc.gov/arthritis/basics/osteoarthritis.htm. Accessed [06 01 2014].

3. Murphy L, Helmick CG."The impact of osteoarthritis in the United States: a population-health perspective." *Am J Nurs*. 3.1 (2012): S13-9.

4. Buckwalter JA, Saltzman C, Brown T. The impact of osteoarthritis. *Clin Orthoped Rel Res*.(2004):427S: S6-S15.

5. Segal, Neil A., Elizabeth R. Boyer, Patricia Teran-Yengle, Natalie A. Glass, Howard J. Hillstrom, and H. John Yack. "Pregnancy Leads to Lasting Changes in Foot Structure." *American Journal of Physical Medicine & Rehabilitation* 92.3 (2013): 232-40.

6. Segal, Neil A., David T. Felson, James C. Torner, Yanyan Zhu, Jeffrey R. Curtis, Jingbo Niu, and Michael C. Nevitt. "Greater Trochanteric Pain Syndrome: Epidemiology and Associated Factors." *Archives of Physical Medicine and Rehabilitation* 88.8 (2007): 988-92.

7. Felson DT, Zhang Y, Hannan MT, Naimark A, Weissman B, Aliabadi P et al.: Risk factors for incident radiographic kneeosteoarthritis in the elderly: the Framingham Study. Arthritis Rheum 1997;40(4):728-33.

8. Anderson, Donald D., Krishna S. Iyer, Neil A. Segal, John A. Lynch, and Thomas D. Brown. "Implementation of Discrete Element Analysis for Subject-Specific, Population-Wide Investigations of Habitual Contact Stress Exposure." *Journal of Applied Biomechanics*26.2 (2010): 215-23.

9. DiMaggio, J. "The Role of Feet and Footwear in Medicolegal Investigations."*Forensic Medicine of the Lower Extremity: Human Identification and Trauma Analysis of the Thigh, Leg, and Foot*. Totowa, NJ: Humana, 2005.

10. Ledoux, William R., and Howard J. Hillstrom. "The Distributed Plantar Vertical Force of Neutrally Aligned and Pes Planus Feet." Gait & Posture 15.1 (2002): 1-9.

11. Cubukcua, S., M. Alimoglub, N. Balcia, and M. Beyazova. "Plantar Arch Type and Strength Profile of the Major Ankle Muscle Groups: A Morphometric-Isokinetic Study." *Isokinetics and Exercise Science* 13 (2005): 217-22.

12. Morris, Henry. "Bones of the Foot." *Morris's Human Anatomy*. Philadelphia: P. Blakiston's Son, 1907. 251-53.

13. Morag, E., and P.r. Cavanagh. "Structural and Functional Predictors of Regional Peak Pressures under the Foot during Walking." *Journal of Biomechanics* 32.4 (1999): 359-70.

14. Hicks, J. H. "The Mechanics of the Foot: II. The Plantar Aponeurosis and the Arch." *Journal of Anatomy* 88.1 (1954): 25-31.

15. Kim, Wangdo, and Arkady S. Voloshin. "Role of Plantar Fascia in the Load Bearing Capacity of the Human Foot." *Journal of Biomechanics* 28.9 (1995): 1025-033.

16. Roxas, Mario. "Plantar Fasciitis: Diagnosis and Therapeutic Considerations."*Alternative Medicine Review* 10.2 (2005): 83-93.

17. Wong, Kevin M. "Dr Kevin M Wong Bunion Aid Foot Problem Expert Alpha Orthotics." *Alpha Orthotics*. Available: http://www.alphaorthotics.com/pages/dr-kevin-m-wong-bunion-aid-foot-problem-expert. [Accessed 04 38 2014].

18. Vullo, VJ, Richardson JK, and EA Hurvitz. "Hip, Knee, and Foot Pain During Pregnancy and the Postpartum Period." *Journal of Family Practice* (1996): 43-63.

19. Wearing, Scott, Andrew Hills, Nuala Byrne, Ewald Hennig, and Michael McDonald. "The Arch Index: A Measure of Flat Feet or Fat Feet?" *Foot & Ankle International* 25.8 (2004): 575-81.

20. Bohemen, E. K., and N. S. T. Gendi. "Flatfeet in Pregnancy." Rheumatology 35.4 (1996): 396-97.

21. Marnach, Mary L., Ramin, Kirk D., Ramsey, Patrick S., Song, Seak-Whan, Stensland, Jacqueline J., and Kai-Nan An. "Characterization of the Relationship between Joint Laxity and Maternal Hormones in Pregnancy." Obstetrics & Gynecology 101.2 (2003): 331-35.

22. Schauberger, C., B. Rooney, L. Goldsmith, D. Shenton, P. Silva, and A. Schaper. "Peripheral Joint Laxity Increases in Pregnancy but Does Not Correlate with Serum Relaxin Levels." American Journal of Obstetrics and Gynecology 174.2 (1996): 667-71.

23. Alvarez, R., A. F. Stokes, D. E. Asprinio, S. Trevino, and T. Braun. "Dimensional Changes of the Feet in Pregnancy." The Journal of Bone and Joint Surgery 70-A.2 (1988): 271-74.

24. Nyska, M., D. Sofer, A. Porat, C. B. Howard, and I. Meizner. "Plantar Foot Pressures in Pregnant Women." *Israel Journal of Medical Sciences* 33.2 (1997): 139-46.

25. Bani, Daniele. "Relaxin: A Pleiotropic Hormone." General Pharmacology: The Vascular System 28.1 (1997): 13-22.

26. Gross, K. Douglas, David T. Felson, Jingbo Niu, David J. Hunter, Ali Guermazi, Frank W. Roemer, Alyssa B. Dufour, Rebekah H. Gensure, and Marian T. Hannan. "Association of Flat Feet with Knee Pain and Cartilage Damage in Older Adults."*Arthritis Care & Research* 63.7 (2011): 937-44.

27. Donatelli, Robert. "Abnormal Biomechanics of the Foot and Ankle." *Journal of Orthopaedic & Sports Physical Therapy* 9.1 (1987): 11-16.

28. Levinger, Pazit, Menz, Hylton B., Fotoohabadi, Mohammad R., Feller, Julian A., Bartlett, John R., and Neil R. Bergman. Foot Posture in People with Medial Compartment Knee Osteoarthritis. Journal of Foot and Ankle Research 2010. 3:29.

29. Blackburn, Turner A., and Emily Craig. "Knee Anatomy: A Brief Review." *Journal of the American Physical Therapy Association* 60.12 (1980): 1556-560.

30. Chhabra, Anikar, C. Curtis Elliott, and Mark D. Miller. "Normal Anatomy and Biomechanics of the Knee." *Sports Medicine and Arthroscopy Review* 9.3 (2001): 166-77.

31. "Common Ailments." Physiotheriapy in Kenilworth. Available from: http://warwickphysio.com/ailments.php?page=16. [Accessed 02 11 2014].

32. Brantigan, Otto C., and Allen F. Voshell. "The Mechanics of the Ligaments and Menisci of the Knee Joint." Journal of Bone and Joint Surgery 23.1 (1941): 44-66.

33. Trimble, Mark H., Mark D. Bishop, Bernadette D. Buckley, Laura C. Fields, and Gerard D. Rozea. "The Relationship between Clinical Measurements of Lower Extremity Posture and Tibial Translation." *Clinical Biomechanics*17.4 (2002): 286-90.

34. Coplan, Julie Angle. "Rotational Motion of the Knee: A Comparison of Normal and Pronating Subjects." *Journal of Orthopaedic & Sports Physical Therapy* 10.9 (1989): 366-69.

35. Rubin, Gustav. "Tibial Rotation." *Bulletin of Prosthetics Research—* (1971): 95-101.

36. Zifchock, Rebecca A., Irene Davis, Howard Hillstrom, and Jinsup Song. "The Effect of Gender, Age, and Lateral Dominance on Arch Height and Arch Stiffness." *Foot & Ankle International* 27.5 (2006): 367-72.

37. "Ankle Anatomy." *Of the Ankle Joint*. 2011. Available: http://www.eorthopod.com/content/ankle-anatomy. [Accessed 05 12 2014].

38. Vieira, Eduardo Luís Cruells, Eduardo Álvaro Vieira, Rogério Teixeira Da Silva, Paulo Augusto Dos Santos Berlfein, Rene Jorge Abdalla, and Moisés Cohen. "An Anatomic Study of the Iliotibial Tract." *Arthroscopy: The Journal of Arthroscopic & Related Surgery* 23.3 (2007): 269-74.

39. Rouse, Simon J. "The Role of the Iliotibial Tract in Patellofemoral Pain and Iliotibial Band Friction Syndromes." *Physiotherapy* 82.3 (1996): 199-202.

40. Ireland, Mary Lloyd, John D. Willson, Bryon T. Ballantyne, and Irene Mcclay Davis. "Hip Strength in Females With and Without Patellofemoral Pain."*Journal of Orthopaedic & Sports Physical Therapy* 33.11 (2003): 671-76.

41. Kwak, S. D., C. S. Ahmad, T. R. Gardner, R. P. Grelsamer, J. H. Henry, L. Blankevoort, G. A. Ateshian, and V. C. Mow. "Hamstrings and Iliotibial Band Forces Affect Knee Kinematics and Contact Pattern." *Journal of Orthopaedic Research* 18.1 (2000): 101-08.

42. Lavine, Ronald. "Iliotibial Band Friction Syndrome." *Current Reviews in Musculoskeletal Medicine* 3.1-4 (2010): 18-22.

43. Khaund, Razib, and Sharon Flynn. "Iliotibial Band Syndrome: A Common Source of Knee Pain." *American Family Physician* 71.8 (2005): 1545-1550.

44. Lee, Thay Q., Garrett Morris, and Rick P. Csintalan. "The Influence of Tibial and Femoral Rotation on Patellofemoral Contact Area and Pressure." *Journal of Orthopaedic & Sports Physical Therapy* 33.11 (2003): 686-93.

45. Powers, Christopher M. "The Influence of Altered Lower-Extremity Kinematics on Patellofemoral Joint Dysfunction: A Theoretical Perspective." *Journal of Orthopaedic & Sports Physical Therapy* 33.11 (2003): 639-46.

46. "ITBS." *RunningPhysio*. N.p., n.d. Web. Available from: http://www.running-physio.com/itbs. Accessed [07 07 2014].

47. Zantop, T., M. Herbort, M. J. Raschke, F. H. Fu, and W. Petersen. "The Role of the Anteromedial and Posterolateral Bundles of the Anterior Cruciate Ligament in Anterior Tibial Translation and Internal Rotation." *The American Journal of Sports Medicine* 35.2 (2006): 223-27.

48. Blecher, Am, and Jc Richmond. "Transient Laxity of an Anterior Cruciate Ligament-reconstructed Knee Related to Pregnancy." *Arthroscopy: The Journal of Arthroscopic & Related Surgery* 14.1 (1998): 77-79.

49. Williams, Bryan S., and Steven P. Cohen. "Greater Trochanteric Pain Syndrome: A Review of Anatomy, Diagnosis and Treatment." *Anesthesia & Analgesia* 108.5 (2009): 1662-670.

50. "Rotational Deformities in Children." *Rotational Deformities of the Legs and Feet in Children*. Available from: http://www.eorthopod.com/content/rotational-deformities-in-children. Accessed [06 21 2014].

51. Felson, D.T., R.C. Lawrence, P.A. Dieppe, R. Hirsch, C.G. Helmick, J.M. Jordan, R.S. Kington, N.E. Lane, M.C. Nevitt, Y. Zhang, M. Sowers, T. McAlindon, T.D. Spector, A.R. Poole, S.Z. Yanovski, G. Ateshian, L. Sharma, J.A. Buckwalter, K.D. Brandt, and J.F. Fries, Osteoarthritis: new insights. Part 1: the disease and its risk factors. Ann Intern Med, 2000. **133**(8): p. 635-46.

52. Buckwalter JA, Brown TD. Joint injury, repair, and remodeling: Roles in post-traumatic osteoarthritis.Clinical Orthopaedics and Related Research 2004;423:7–16.

53. Srikanth, et al. "A Meta-analysis of Sex Differences Prevalence, Incidence and Severity of Osteoarthritis1." Osteoarthritis and Cartilage 13.9 (2005): 769-81.

54. Tonelli et al. "Women with knee osteoarthritis have more pain and poorer function than men, but similar physical activity prior to total knee replacement." Biology of Sex Differences 2011 2:12.

55. Ringdahl, Erika, and Sandesh Pandit. "Treatment of Knee Osteoarthritis." *Journal of American Family Physician* 83.11 (2011): 1287-292.

56. Andriacchi, Thomas P., Anne Mündermann, R. Lane Smith, Eugene J. Alexander, Chris O. Dyrby, and Seungbum Koo. "A Framework for the in Vivo Pathomechanics of Osteoarthritis at the Knee." *Annals of Biomedical Engineering* 32.3 (2004): 447-57.

57. Segal, Neil A., Donald D. Anderson, Krishna S. Iyer, Jennifer Baker, James C. Torner, John A. Lynch, David T. Felson, Cora E. Lewis, and Thomas D. Brown. "Baseline Articular Contact Stress Levels Predict Incident Symptomatic Knee Osteoarthritis Development in the MOST Cohort." Journal of Orthopaedic Research (2009).

58. Bei, Yanhong, and Benjamin J. Fregly. "Multibody Dynamic Simulation of Knee Contact Mechanics." *Medical Engineering & Physics* 26.9 (2004): 777-89.

59. Li, Guoan, Makoto Sakamoto, and Edmund Y.S. Chao. " A Comparison of Different Methods in Prediction Static Pressure Distribution in Articulating Joints." *Journal of Biomechanics* 30.6 (1997): 635-38

60. Chao, E.Y., et al. "Discrete element analysis in musculoskeletal biomechanics." *Molecular & cellular biomechanics* **7**.3 (2010): 175-92.

61. Schuind, F., W.p. Cooney, R.l. Linscheid, K.n. An, and E.y.s. Chao. "Force and Pressure Transmission through the Normal Wrist. A Theoretical Two-dimensional Study in the Posteroanterior Plane." *Journal of Biomechanics*28.5 (1995): 587-601.

62. Fregly, B.J., et al. "Computational wear prediction of a total knee replacement from in vivo kinematics." *Journal of biomechanics* 38.2 (2005): 305-14.

63. Blankevoort, L., J.h. Kuiper, R. Huiskes, and H.j. Grootenboer. "Articular Contact in a Three-dimensional Model of the Knee." *Journal of Biomechanics* 24.11 (1991): 1019-031.

64. Halloran, Jason P., Sarah K. Easley, Anthony J. Petrella, and Paul J. Rullkoetter. "Comparison of Deformable and Elastic Foundation Finite Element Simulations for Predicting Knee Replacement Mechanics." *Journal of Biomechanical Engineering* 127.5 (2005): 813.

65. Butler, Robert J., Howard Hillstrom, Jinsup Song, Christine Richards, and Irene S. Davis. "Arch Height Index Measurement System: Establishment of Reliability and Normative Values." *Journal of the American Podiatric Medical Association* 98.2 (2008): 102-06.

66. Grood, E. S., and W. J. Suntay. "A Joint Coordinate System for the Clinical Description of Three-Dimensional Motions: Application to the Knee."*Journal of Biomechanical Engineering* 105.2 (1983): 136.

67. Fregly, Benjamin J., Thor F. Besier, David G. Lloyd, Scott L. Delp, Scott A. Banks, Marcus G. Pandy, and Darryl D. D'lima. "Grand Challenge Competition to Predict in Vivo Knee Loads." *Journal of Orthopaedic Research* 30.4 (2012): 503-13.

68. Hrdlicka, Ales. "Study of the Normal Tibia." *American Anthropologist* 11.10 (1898): 307-12.

69. Fukubayashi, Toru, and Hlsashi Kurosawa. "The Contact Area and Pressure Distribution Pattern of the Knee."*Acta Orthopaedica* 51.1-6 (1980): 871-79.

70. Walker, P. S., and M. J. Erkman. "The Role of the Meniscus in Force Transmission Across the Knee."*Clinical Orthopaedics* 106 (1975): 184-92.

71. Guess, Trent M., Hongzeng Liu, Sampath Bhashyam, and Ganesh Thiagarajan. "A Multibody Knee Model with Discrete Cartilage Prediction of Tibio-femoral Contact Mechanics." *Computer Methods in Biomechanics and Biomedical Engineering* (2011): 1-15.